NASA Technical Paper 1862

Stress-Concentration Factors for Finite Orthotropic Laminates With a Pin-Loaded Hole

John H. Crews, Jr., C. S. Hong,
and I. S. Raju

MAY 1981

NASA

NASA Technical Paper 1862

Stress-Concentration Factors for Finite Orthotropic Laminates With a Pin-Loaded Hole

John H. Crews, Jr., and C. S. Hong
Langley Research Center
Hampton, Virginia

I. S. Raju
The George Washington University
Joint Institute for Advancement of Flight Sciences
Langley Research Center
Hampton, Virginia

National Aeronautics
and Space Administration

**Scientific and Technical
Information Branch**

1981

SUMMARY

Stresses were calculated for finite-size orthotropic laminates loaded by a frictionless steel pin in a circular hole of the same diameter. These calculations were based on finite-element analyses for six laminates: quasi-isotropic $[0^{\circ}/\pm45^{\circ}/90^{\circ}]_s$, 0°, 90°, $[0^{\circ}/90^{\circ}]_s$, $[\pm45^{\circ}]_s$, and $[0^{\circ}/\pm45^{\circ}]_s$. Stress concentration factors, based on nominal bearing stress, were determined for wide ranges of the ratios of width to diameter w/d and edge distance to diameter e/d. For reference purposes, the infinite-laminate case was also analyzed for each laminate.

Orthotropy had a significant influence on both the magnitude and location of the maximum tensile stress concentration on the boundary of the hole. For example, the stress-concentration factors for the infinite-laminate cases ranged from 0.82 to 2.16, compared with 0.87 for the quasi-isotropic laminate. The laminates with 0° plies developed the peak tensile stress near the ends of the pin/hole contact arc. But the 90° and $\pm45^{\circ}$ laminates had peaks where ply fibers were tangent to the hole.

The finite widths and edge distances strongly influenced the tensile stress concentration. For the practical range $w/d \geq 3$, the peak tensile stresses were as much as 80 percent larger than the infinite-laminate reference value. Even for rather wide laminates with $w/d = 10$, some of the peak tensile stresses were amplified by nearly 20 percent. For $e/d \geq 3$, these stresses were amplified by as much as 50 percent. In contrast, the finite width and edge distance had little effect on shear-out and bearing stress concentrations. For $w/d \geq 3$ and $e/d \geq 3$, the peak shear-out stress was amplified by less than 25 percent and peak bearing stress by only 10 percent.

INTRODUCTION

The stress concentrations at fastener holes are widely recognized as having a degrading effect on structural fatigue life. In conventional metallic structures, fatigue cracks commonly initiate at these stress-concentration sites. In recognition of this, the effects of stress concentrations on crack initiation and growth have been incorporated into current methods for predicting fatigue life. However, in composite structures, the stress concentration effects are much more complicated and are not well understood. For example, holes can produce either composite delamination, matrix crazing, fiber failures, or various combinations of these. Furthermore, for a pin-loaded hole, these different types of damage can produce three different modes of failure: net-tension, shear-out, or bearing. Before analytical models can be developed for these various failures, the stress concentrations at loaded holes must be better understood. To date, the few stress analyses that have dealt with this problem have been limited to rather specific cases. The purpose of the present paper is to present some of the needed background on stresses at loaded holes in composite laminates.

This study was based on a two-dimensional finite-element analysis of stresses in an orthotropic laminate that is loaded by a frictionless steel pin in a circular hole of the same diameter. Six graphite/epoxy laminates were analyzed: quasi-isotropic $[0^o/\pm45^o/90^o]_s$, 0^o, 90^o, $[0^o/90^o]_s$, $[\pm45^o]_s$, and $[0^o/\pm45^o]_s$. Finite-element models were developed for wide ranges of width-to-diameter ratio w/d and edge-distance-to-diameter ratio e/d. First, each laminate was analyzed for different values of w/d using one large value of e/d. Next, a range of e/d was used with one large w/d value.

The results are presented in two ways: first as stress distributions near the hole and then as stress-concentration factors for ranges of w/d and e/d. Results for the orthotropic laminates were compared with the quasi-isotropic laminate which served as a reference case. Similarly, the w/d and e/d effects were evaluated relative to an infinite-laminate reference case.

SYMBOLS

d	diameter of hole, m
E_{xx}, E_{yy}	Young's modulus in x- and y-directions, respectively, MPa
e	edge distance, m
G_{xy}	shear modulus, MPa
K_{sb}	shear stress-concentration factor, $(\tau_{xy})_{max}/S_b$
$(K_{sb})_\infty$	K_{sb} for an infinite laminate
K_{tb}	tensile stress-concentration factor, $(\sigma_{\theta\theta})_{max}/S_b$
$(K_{tb})_\infty$	K_{tb} for an infinite laminate
K_{tg}	gross-section stress-concentration factor, $(\sigma_{\theta\theta})_{max}/S_g$
P	pin load, N
R	radius of hole, m
r, θ	polar coordinates, m and deg
S_b	nominal bearing stress, P/td, MPa
S_g	nominal gross-section stress, MPa
t	laminate thickness, m
w	width of laminate, m
x, y	Cartesian coordinates, m

θ_c	one-half the angle of contact between pin and hole, deg
θ_m	angular location for $(\sigma_{\theta\theta})_{max}$ on hole boundary, deg
ν_{xy}	Poisson's ratio
σ	stress, MPa
$\sigma_{rr}, \sigma_{\theta\theta}$	polar stress components, MPa
$(\sigma_{\theta\theta})_{max}$	maximum tangential stress on hole boundary, MPa
τ_{xy}	Cartesian shear stress, MPa
$(\tau_{xy})_{max}$	maximum τ_{xy} on shear-out plane (y = R), MPa

FINITE-ELEMENT ANALYSIS

Figure 1 shows the general problem analyzed in this study. The laminate had a frictionless hole which was loaded by a steel pin of the same diameter. The laminate reacted to the pin load by a uniform stress on its left end. The hole diameter was unity and the various combinations of w/d and e/d were generated by varying w and e in the finite-element models. The w/d effects were analyzed using a single, large value of e/d (e/d = 10). Similarly, the e/d effects were studied using w/d = 20. For all cases, the hole was at a distance of 10d from the left (loaded) end of the laminate.

Table I presents the elastic constants for the six laminates analyzed. These laminates were selected to cover a broad range of composite properties. The 0^o laminate properties (ref. 1) were used with laminate theory to calculate the elastic constants for the other laminates. Although the $[0^o/\pm45^o/90^o]_s$ laminate was called a quasi-isotropic laminate, its calculated elastic constants satisfy all the criteria for isotropy. Consequently, the results for the quasi-isotropic case were compared with isotropic solutions from the literature as a check on the adequacy of the finite-element analysis.

The finite-element model for one-half of a 20d by 20d square laminate is shown in figure 2. To illustrate the model details, it is shown in four parts. This was the largest model analyzed (w/d = 20 and e/d = 10). Smaller values of w/d and e/d were obtained by removing elements from the width and unloaded end of the model, respectively. This model employed two types of finite elements. Linear-strain (6-node) elements comprised the 2.5d by 5d rectangular region around the hole. Uniform-strain (3-node) elements comprised the part of the model outside this region. The model was analyzed using the BEND finite-element computer program described in reference 2.

Note that the pin is also modeled in figure 2. The pin was loaded at its center and was connected to the laminate by short, stiff spring elements (0.002d long) between adjacent nodes across the pin/laminate interface. Because these springs had no transverse stiffness, they transferred only radial loads

and thereby produced the desired frictionless interface. Also, these springs were used to allow the pin and laminate to separate along part of their interface. This was accomplished by assigning a zero stiffness to springs along the separation arc. References 3 and 4 show that this separation was independent of loading level for the special case of an initially snug fit (zero clearance) between the pin and laminate. For this reason, a snug fit was used in the present study. For each combination of material and configuration, the separation angle was estimated and a computer run was made. When a spring was computed to have a tensile force, its stiffness was set equal to zero and that case was rerun. Such reruns were needed for only a few cases.

RESULTS AND DISCUSSION

Evaluation of Finite-Element Procedure

The finite-element procedure was evaluated by comparing results for the quasi-isotropic laminate with results in the literature for an isotropic, infinite sheet containing a rigid pin with a snug fit. The appendix describes the present finite-element analysis used to approximate this infinite-sheet case. The results for this special case are presented in figure 3 as stress distributions around the hole. The stresses are normalized by the nominal bearing stress S_b, which is defined as P/td, where P is the pin load, t is the laminate thickness, and d is the hole diameter.

Figure 3 also includes a curve for $\sigma_{rr} = -4/\pi \cos \theta$ because several authors have assumed this cosine distribution for bearing stress, either directly or indirectly, by assuming a rigid-body displacement for the pin. The present results (solid curve) and the results of reference 5 (dashed curve) are in general agreement with the cosine distribution, except for the angle of contact between the pin and the laminate. The 90° contact angle θ_c for the cosine distribution is slightly larger than the 83° contact angle found in the present study and in references 3 and 5.

The $\sigma_{\theta\theta}$ curves reach a peak $(\sigma_{\theta\theta})_{max}$ near the end of the contact arc. This peak was represented by a tensile stress-concentration factor K_{tb}. In references 6 and 7, it was assumed that $\theta_c = 90^\circ$, and K_{tb} was calculated as 0.81. In references 3 and 5, however, K_{tb} was calculated as 0.92 and 0.91, respectively, when $\theta_c = 83^\circ$ was used. As shown in figure 3, these results bracket the present K_{tb} of 0.87. In general, the present results agree reasonably well with the available solutions for pin-loaded holes in isotropic sheets.

As an additional check on the present finite-element model, stresses were computed for an open hole (zero bolt modulus) in a sheet under remote uniaxial tension. For isotropic material properties, a gross-section stress-concentration factor K_{tg} of 3.01 was calculated, compared with the familiar value of 3.00 for an infinite sheet. For the extreme case of 0° laminate properties, $K_{tg} = 6.45$, which compares favorably with the infinite-sheet value of 6.43 from reference 8.

Width Effects

As previously mentioned, six laminates were analyzed. The w/d values ranged from 2 to 20 and e/d was 10. For each case, the laminate was loaded by a steel pin having a snug fit. Results are first presented as stress distributions near the hole and are briefly discussed in terms of the basic failure modes: net-tension, shear-out, and bearing. Next, stress-concentration factors are plotted for a range of w/d values. Finally, these stress-concentration factors are compared with their corresponding infinite-laminate values. The quasi-isotropic laminate serves as a reference case to evaluate the effects of anisotropy.

Stress distributions.- Stresses for the quasi-isotropic laminate are shown in figure 4. For simplicity, only results for $w/d = 2$, 3, and ∞ are shown; other results for the full w/d range are summarized in table II. In figure 4(a), the $\sigma_{\theta\theta}$ curve for $w/d = 2$ has a maximum value $(\sigma_{\theta\theta})_{max}$ that is more than twice that for $w/d = \infty$. In contrast, the σ_{rr} curves show only minor differences for the various w/d values. In fact, the maximum σ_{rr} is nearly unaltered, and the contact angle θ_c varies only from about 83^o to 90^o. Figure 4(b) shows the shear stress τ_{xy} computed for the shear-out failure plane, $y = R$. The narrow laminate width of $w/d = 2$ elevated this τ_{xy} by about 25 percent above the infinite-laminate case.

The $\sigma_{\theta\theta}$, σ_{rr}, and τ_{xy} in figure 4 are associated, respectively, with the following failure modes: net-tension, shear-out, and bearing. Of these, only $\sigma_{\theta\theta}$ shows much dependence on w/d. As a result, only the net-tension failure strength should be strongly influenced by laminate width.

The 0^o laminate stresses are presented in figure 5. The $\sigma_{\theta\theta}$ curves for this highly orthotropic case have larger maximum values and larger gradients than for the quasi-isotropic case. However, $(\sigma_{\theta\theta})_{max}$ for $w/d = 2$ is only about twice as large as the corresponding value for $w/d = \infty$; this w/d effect is comparable to that found for the quasi-isotropic laminate. The σ_{rr} curves differ markedly from the cosine distribution and have a sharp peak at $\theta = 0^o$, which is the stiffest direction for this 0^o laminate. The σ_{rr} curves have almost no dependence on w/d and show a contact angle θ_c of about 82^o. The τ_{xy} curves are also only slightly different for the range of w/d values.

Results for the 90^o laminate are presented in figure 6. Although the $\sigma_{\theta\theta}$ curves have the expected peaks near $\theta = 90^o$, they have higher peaks at $\theta = 0^o$. Note that in this 90^o laminate the fibers are tangent to the hole at the point of maximum $\sigma_{\theta\theta}$. Again, the σ_{rr} curves are quite similar to one another; all deviate from the cosine distribution. Also, they deviate significantly from the two previous laminates by having their maxima near $\theta = 70^o$. The contact angles in figure 6 range from about 84^o to 86^o. The τ_{xy} curves in figure 6 have higher peaks than those found for the two previous laminates.

The $[0^o/90^o]_s$ laminate results are plotted in figure 7. As expected, these results are approximately equal to averages of those shown for 0^o and 90^o laminates. The $(\sigma_{\theta\theta})_{max}$ value for $w/d = 2$ is located at $\theta = 90^o$ and is about twice as large as its infinite-laminate value. The σ_{rr} curves and the τ_{xy} curves are like those for the quasi-isotropic case in figure 4.

The stress distributions for the $[\pm 45]_s$ laminate, plotted in figure 8, are unlike those in previous figures. The $\sigma_{\theta\theta}$ curve for $w/d = \infty$ has a pronounced peak at $\theta = 45^o$, where the -45^o ply fibers are tangent to the hole. For smaller w/d values, the $\sigma_{\theta\theta}$ curves have a second peak near $\theta = 135^o$ where the 45^o ply fibers are tangent to the hole. This second peak appears to be strongly amplified for narrow laminates. Furthermore, narrow laminates show larger contact angles and larger stresses near the end of the contact arc than wide laminates.

The $[0^o/\pm 45^o]_s$ results shown in figure 9 have the expected trends. For small w/d values, $(\sigma_{\theta\theta})_{max}$ is nearly three times the infinite-laminate value. This peak value occurs slightly beyond the region of contact. The σ_{rr} and τ_{xy} curves are similar to the quasi-isotropic results and are not strongly influenced by the laminate width.

Stress-concentration factors.- To compare the six different laminates, the stress-concentration factor K_{tb} was calculated using each value of $(\sigma_{\theta\theta})_{max}$ in the previous figures. These K_{tb} values are listed in table II along with the location θ_m for each value of $(\sigma_{\theta\theta})_{max}$ and the contact angle θ_c that occurred for each case. The K_{tb} values are also plotted in figure 10 for the range $2 \leqq w/d \leqq 10$. This figure shows similar width effects for all six laminates; the larger w/d values produced smaller K_{tb} values. As previously mentioned, the quasi-isotropic case provides a reference for evaluating the anisotropy effects. The curve for this reference case lies near the lower extreme for the range of computed results. Only the $[0^o/\pm 45^o]_s$ curve is lower. Note that the results from reference 9 for a finite-width isotropic sheet agree closely with the present quasi-isotropic results. As expected, the 0^o laminate curve is the upper bound for the range of results, and the $[0^o/90^o]_s$ curve lies near the middle of this range. Comparisons involving the 90^o laminate and the $[\pm 45^o]_s$ laminate are difficult because their $(\sigma_{\theta\theta})_{max}$ values occurred at $\theta_m = 0^o$ and 45^o, respectively, rather than at the usual $\theta_m \approx 90^o$ for the laminates containing some 0^o plies.

The curves in figure 10 appear to have a negative slope even at $w/d = 10$, suggesting that the width effects may exist beyond $w/d = 10$. To investigate this, the K_{tb} values were each normalized by their corresponding infinite-laminate value $(K_{tb})_\infty$ and then replotted in figure 11. Of the six curves in figure 11, only those for the 90^o laminate and the $[\pm 45^o]_s$ laminate approach unity, indicating that only for these laminates is the effect negligible for $w/d = 10$. The other four curves converge to about 1.17. This means that K_{tb} is amplified by 17 percent even for a rather wide plate with $w/d = 10$. For comparison, if the present laminates had unloaded holes and remote uniaxial loads, their stress concentrations would be amplified by less than about 2 percent at $w/d = 10$ (ref. 10). This comparison shows that a finite width influences the tensile stress concentration at a loaded hole much more than it does for an unloaded hole. In figure 11, the curves for all the laminates that contain some 0^o plies lie close to the quasi-isotropic reference curve. In fact, for $w/d \geqq 3$, use of the quasi-isotropic curve to approximate the others with 0^o plies would result in errors of less than 10 percent. The other two laminates, 90^o and $[\pm 45^o]_s$, have curves in figure 11 that lie well below that for the quasi-isotropic case. However, these two laminates have their peak values at $\theta_m = 0^o$ and 45^o, respectively.

Edge-Distance Effects

As previously described, the six laminates were analyzed for edge-distance effects by using a value of $w/d = 20$. The e/d values ranged from 1 to 20. The laminates were assumed to be loaded by a steel pin fitting snugly in the hole. First, the results are plotted as stress distributions for each laminate. The stress-concentration factors for the six laminates are then compared with one another and with their corresponding infinite-laminate values.

Stress distributions.- The quasi-isotropic case was again used as a reference to investigate the effects of laminate anisotropy on stresses at a loaded hole. Stress distributions for the quasi-isotropic case are presented in figure 12. The curves for two finite edge distances ($e/d = 1$ and 2) are shown along with those for an infinite laminate ($e/d = \infty$). For the extreme $e/d = 1$ case in figure 12(a), the peak $\sigma_{\theta\theta}$ is about twice as large as that for $e/d = \infty$. As expected, this peak occurs near the end of the contact arc. But for small e/d values, this peak shifts slightly to the left, in contrast to figure 4(a), which shows a slight shift to the right for small w/d values. Otherwise, however, the $\sigma_{\theta\theta}$ trends in figure 12(a) are quite similar to those in figure 4(a). The σ_{rr} and τ_{xy} curves in figures 12(a) and 12(b) show little influence of e/d, as long as $e/d \geq 2$.

Figure 13 presents stresses computed for the 0° laminate. This extremely orthotropic laminate is strongly influenced by finite edge distances. Even for $e/d = 2$, figure 13(a) shows that $(\sigma_{\theta\theta})_{max}$ is about twice as large as for the reference case ($e/d = \infty$). For $e/d = 1$, it is about three times as large. (See table III.) This stress amplification due to finite e/d values is larger than that shown in the previous section for finite w/d values. This is probably attributable to the fact that the 0° laminate is very stiff in the edge-distance direction but very flexible in the width direction. In contrast to the $\sigma_{\theta\theta}$ curves, the σ_{rr} curves show very little e/d influence; the contact angle θ_c is about 82° for the full range of e/d values.

Figure 13(b) shows that e/d has a strong influence on the τ_{xy} values computed for the shear-out plane ($y = R$). The τ_{xy} curve for $e/d = 1$ has a peak that is about three times as large as the infinite-laminate value. The $(\tau_{xy})_{max}$ values are similar for both the 0° and quasi-isotropic laminates. Of course, these laminates have different shear strengths and therefore should respond differently to the same τ_{xy} stress. For example, the 0° laminate has a shear strength that is only about one-fourth that for the quasi-isotropic case and is therefore more vulnerable to the shear-out failure mode.

The 90° laminate stresses are plotted in figure 14. All three stresses show relatively little influence of e/d. These stresses were increased by only about 50 percent even for the extreme $e/d = 1$ case. Perhaps this laminate shows little sensitivity to the free edge because it has a very low stiffness in the edge-distance (x-axis) direction.

The $[0^\circ/90^\circ]_s$ laminate is relatively stiff in the x-direction and, as expected, has a much stronger dependence on e/d than observed for the 90° laminate. For $e/d = 1$ (fig. 15), the $(\sigma_{\theta\theta})_{max}$ is about twice as large as when $e/d = \infty$. Also, $(\sigma_{\theta\theta})_{max}$ occurs at $\theta = 0^\circ$ for this $e/d = \infty$

reference case but occurs at $\theta = 90^{\circ}$ for finite edge distances. Similarly, the σ_{rr} peak occurs at $\theta = 0^{\circ}$ for $e/d = \infty$ but shifts toward $\theta = 45^{\circ}$ for finite e/d values.

Figures 16 and 17 present stress distributions for the $[\pm 45^{\circ}]_s$ and the $[0^{\circ}/\pm 45^{\circ}]_s$ laminates, respectively. As expected, the $[\pm 45^{\circ}]_s$ curves in figure 16(a) have their peak value at $\theta = 45^{\circ}$, where the -45° ply fibers are tangent to the hole. This highly stressed -45° ply is probably responsible for the relatively large τ_{xy} peak shown in figure 16(b). The $\sigma_{\theta\theta}$ curves for the $[0^{\circ}/\pm 45^{\circ}]_s$ laminate have their peak at the usual $\theta = 90^{\circ}$ location. In fact, all the $[0^{\circ}/\pm 45^{\circ}]_s$ results in figure 17 are quite similar to the $[0^{\circ}/\pm 45^{\circ}/90^{\circ}]_s$ reference case in figure 12. Apparently, the 90° plies have little influence on the stresses near a loaded hole when they are used together with 0° and $\pm 45^{\circ}$ plies.

Stress-concentration factors.- Stress-concentration factors K_{tb} for the six laminates are compared for a range of e/d in figure 18. These K_{tb} values were calculated using $(\sigma_{\theta\theta})_{max}$ from $\sigma_{\theta\theta}$ stress distributions. These K_{tb} values are also presented in table III, along with the contact angle θ_c and the angular location θ_m for each case. Figure 18 shows that, despite the wide range of K_{tb} for $e/d = 1$, all six curves lie within a range of 0.90 to 2.16 for $e/d = 10$. As in the previous analysis for w/d effects, the quasi-isotropic reference curve lies near the lower end of this range. Apparently, the quasi-isotropic laminate provides the most uniform load transfer near a loaded hole. Anisotropy produces more concentrated load paths and correspondingly higher stress concentrations.

Figure 19 presents a comparison of these K_{tb} results in a different way. Each K_{tb} value was normalized by the corresponding $(K_{tb})_{\infty}$ value for that laminate. Each curve in figure 19 should approach unity for sufficiently large e/d values, and they all appear to have this trend. For $e/d = 10$, each curve lies within the narrow range of 1.0 to 1.1. However, for $e/d = 3$, a practical value for bolted joints, the K_{tb} for a quasi-isotropic laminate is about 25 percent larger than for the infinite-laminate case; K_{tb} values for all the other laminates with 0° plies are even larger. The largest increase is about 50 percent for the 0° laminate.

Because shear-out is a viable failure mode for finite e/d cases, stress-concentration factors were also calculated for the τ_{xy} stress along the shear-out planes. Figure 20 shows the stress-concentration factor $K_{sb} = (\tau_{xy})_{max}/S_b$. (Also see table IV.) For $e/d = 1$, the K_{sb} results are rather tightly grouped in the range 0.7 to 0.9. But for larger e/d values, K_{sb} ranges from about 0.2 to 0.6. As expected, the 90° laminate provides the upper bound for this range and the 0° laminate provides the lower bound. The quasi-isotropic curve lies near midrange.

Each K_{sb} was normalized by the corresponding infinite-laminate value $(K_{sb})_{\infty}$. These $K_{sb}/(K_{sb})_{\infty}$ results are shown in figure 21. As expected, for small e/d values, the results have a wide range. But for $e/d \geq 3$, all six curves are closely grouped and approach unity. For $e/d \geq 3$, the e/d effect is less than about 25 percent, even for the extremely orthotropic 0° laminate.

Stress-concentration factors for the σ_{rr} stress were also calculated, but the e/d effects were found to be quite small. For $e/d \geq 3$, the peak σ_{rr} stresses were less than 10 percent larger than corresponding infinite-laminate values. Consequently, e/d should have a negligible effect on bearing strength for $e/d \geq 3$.

CONCLUDING REMARKS

Stresses were calculated for finite-size orthotropic laminates that are loaded by a frictionless steel pin in a circular hole of the same diameter. These calculations were based on finite-element analyses for six laminates: quasi-isotropic $[0^\circ/\pm45^\circ/90^\circ]_s$, 0°, 90°, $[0^\circ/90^\circ]_s$, $[\pm45^\circ]_s$, and $[0^\circ/\pm45^\circ]_s$. Stress-concentration factors were based on nominal bearing stress and were determined for wide ranges of width-to-diameter ratio w/d and edge-distance-to-diameter ratio e/d. For reference purposes, the infinite-laminate case was also analyzed for each laminate.

When load is introduced into a laminate by a pin, the hole surface and pin remain in contact only over a portion of the hole boundary defined by a contact arc. In general, for cases with either an initial clearance fit or an interference fit, this contact arc varies with load. However, recent literature shows that the present case with an initially snug fit has a contact arc that is independent of load. Although each combination of laminate material and configuration produced a different contact arc, each such arc was in the narrow range of 160° to 180°. Therefore, neither the wide ranges of material anisotropy nor laminate configuration had much influence on the contact arc. As expected, anisotropy had a strong influence on the contact stress distributions. These distributions deviated significantly from the well-known cosine distribution, especially for the 0° and 90° laminates.

The anisotropy also had a strong influence on the magnitude and location of the peak tangential stress on the hole boundary. This peak was represented by a stress-concentration factor K_{tb}. For the infinite-laminate case, the stress concentration factor ranged from 0.82 to 2.16 compared to 0.87 for the quasi-isotropic laminate. The stress peak developed near the end of the contact arc except for the 90° and $[\pm45^\circ]_s$ laminates, which had their peaks where the ply directions (fibers) were tangent to the hole.

The narrow laminates produced large K_{tb} values for the loaded holes. Even for a rather wide (w/d = 10) configuration, the quasi-isotropic laminate had a K_{tb} that was nearly 20 percent larger than its infinite-laminate reference value. In contrast, for an unloaded hole, the corresponding stress-concentration factor is only about 2 percent larger than its infinite-laminate value. In general, the orthotropic laminates containing 0° plies produced trends quite like that for the quasi-isotropic laminate, especially for $w/d \geq 3$. Also for $w/d \geq 3$, the peak bearing stresses for all six laminates were elevated by less than about 10 percent.

As expected, the finite-edge distance also increased the stresses near the loaded hole. However, this influence varied widely for the different laminates and different stresses. For the extreme case of e/d = 1, this influence

increased the 0° laminate K_{tb} by more than 200 percent but increased the 90° laminate K_{tb} by only 50 percent. The edge distances only weakly influenced the peak values for shear-out and bearing stress. For $e/d \geqq 3$, the peak shear stresses were increased by less than about 25 percent. Similarly, for $e/d \geqq 3$, the peak bearing stresses were increased by less than 10 percent.

In summary, both finite width and finite edge distance had a strong influence on the maximum tensile stress, but had much less influence on the other peak stresses near the hole.

Langley Research Center
National Aeronautics and Space Administration
Hampton, VA 23665
April 1, 1981

APPENDIX

APPROXIMATION FOR INFINITE-LAMINATE CASE

To analyze the infinite-laminate case, the finite-element procedure was systematically applied for increasing values of w/d. The computed stress-concentration factor K_{tb} for a loaded hole was expected to asymptotically approach an infinite-laminate value $(K_{tb})_\infty$. This ancillary "convergence" study was conducted with a square, quasi-isotropic laminate and, for comparison with the literature, the pin was assumed to be rigid.

Figure 22 and table V present K_{tb} values for the three different loading cases analyzed in the convergence study. Case 1, represented by the upper curve, is the basic problem dealt with in this study. Case 2 is included for comparison purposes. Note that cases 1 and 2 have the remote stress reactions on opposite ends of the model. Otherwise, these two cases are identical and, for an infinite laminate, they should have the same $(K_{tb})_\infty$ value because the remote stress would be zero for both cases. On the other hand, the difference between the K_{tb} curves for cases 1 and 2 is a measure of the finite-size effect for a given w/d value. The curves for cases 1 and 2 converge slowly in figure 22 and differ by almost 20 percent at $w/d = 20$.

Because neither the case 1 curve nor the case 2 curve approached a limit for the present range of w/d, the third case was considered. This case could be generated by superimposing cases 1 and 2. Therefore, if cases 1 and 2 have the same limit, then the limit must also apply to case 3. Conversely, a limit found for case 3 would also be the desired limit for case 1. Toward this end, case 3 loading was used in the finite-element analysis for a range of w/d values. The resulting K_{tb} curve in figure 22 has nearly converged for $w/d = 20$.

To check the assumption that all three curves in figure 22 converge to $(K_{tb})_\infty$, each curve was extrapolated by using a numerical analysis. Each curve was approximated by the cubic polynomial

$$K_{tb} = a_0 + a_1\left(\frac{d}{w}\right) + a_2\left(\frac{d}{w}\right)^2 + a_3\left(\frac{d}{w}\right)^3$$

The coefficients a_0 to a_3 were obtained by a least-squares fit to the K_{tb} values in table V. The polynomials were each found to have a correlation coefficient that deviated from unity by less than 4×10^{-6}, indicating nearly perfect agreement with the tabulated K_{tb} values. For very large w/d values, each polynomial approaches its constant a_0 term. Therefore, each a_0 was an estimate for $(K_{tb})_\infty$. The three a_0 values were 0.863, 0.864, and 0.863, respectively, for cases 1, 2, and 3. Therefore, the three curves converge to the same limit of about 0.863.

APPENDIX

For convenience, the case 3 results for $w/d = 20$ were assumed to approximate the infinite-laminate results for case 1. The resulting value $(K_{tb})_\infty = 0.869$ was considered to be sufficiently close to the 0.863 extrapolated limit. The infinite-laminate stress distributions and $(K_{tb})_\infty$ values for the other laminates were also approximated using case 3 loading with $w/d = 20$. The $(K_{tb})_\infty$ values are presented in table II and, for comparison purposes, are repeated in table III. The shear stress-concentration factors $(K_{sb})_\infty$ for an infinite laminate are presented in table IV.

REFERENCES

1. Advanced Composites Design Guide. Volume I - Design. Third Edition (Second Revision). Contract No. F33615-74-C-5075, Flight Dyn. Lab. U.S. Air Force, Sept. 1976. (Available from DTIC as AD B027 146.)

2. Pifko, A.; Levine, H. S.; and Armen, H., Jr.: PLANS - A Finite Element Program for Nonlinear Analysis of Structures. Volume I - Theoretical Manual. NASA CR-2568, 1975.

3. Eshwar, V. A.; Dattaguru, B.; and Rao, A. K.: Partial Contact and Friction in Pin Joints. Rep. No. ARDB-STR-5010, Dep. Aeronaut. Eng., Indian Inst. Sci., Dec. 1977.

4. Mangalgiri, P. D.; and Dattaguru, B.: Elastic Analysis of Pin Joints in Composite Plates. Rep. No. ARDB-STR-5014, Dep. Aeronaut. Eng., Indian Inst. Sci., 1981. (Available as Mangalgiri, P. D.: Elastic Analysis of Pin Joints in Composite Plates. Ph. D. Thesis, Indian Inst. Sci., Apr. 1980.)

5. DeJong, Theo: Stresses Around Pin-Loaded Holes in Elastically Orthotropic or Isotropic Plates. J. Compos. Mater., vol. 11, July 1977, pp. 313-331.

6. Bickley, W. G.: The Distribution of Stress Round a Circular Hole in a Plate. Philos. Trans. R. Soc. London, ser. A, vol. 227, Aug. 1928, pp. 383-415.

7. Waszczak, John P.: A Synthesis Procedure for Mechanically Fastened Joints in Advanced Composite Materials. Rep. SM-73-11 (Contracts F33615-70-C-1146 and F33615-72-C-1214), Dep. Mech. Eng., Carnegie-Mellon Univ., Apr. 1973.

8. Lekhnitskii, S. G.: Theory of Elasticity of an Anisotropic Elastic Body. Holden-Day, Inc., 1963.

9. Theocaris, P. S.: The Stress Distribution in a Strip Loaded in Tension by Means of a Central Pin. J. Appl. Mech., vol. 23, no. 1, Mar. 1956, pp. 85-90.

10. Hong, C. S.; and Crews, John H., Jr.: Stress-Concentration Factors for Finite Orthotropic Laminates With a Circular Hole and Uniaxial Loading. NASA TP-1469, 1979.

TABLE I.- LAMINATE ELASTIC CONSTANTS

Laminate	Elastic constants			
	E_{xx}, MPa	E_{yy}, MPa	G_{xy}, MPa	ν_{xy}
Quasi-isotropic $[0^o/\pm45^o/90^o]_s$	57 890	57 890	22 090	0.310
0^o	146 900	10 890	6 412	0.380
90^o	10 890	146 900	6 412	0.028
$[0^o/90^o]_s$	79 500	79 500	6 412	0.052
$[\pm45^o]_s$	22 250	22 250	37 770	0.735
$[0^o/\pm45^o]_s$	64 200	28 210	27 320	0.699

TABLE II.- TENSION STRESS-CONCENTRATION FACTORS FOR w/d RANGE WITH e/d = 10

w/d	Quasi-isotropic $[0^\circ/\pm45^\circ/90^\circ]_s$		0°		90°		$[0^\circ/90^\circ]_s$		$[\pm45^\circ]_s$		$[0^\circ/\pm45^\circ]_s$	
	K_{tb}	θ_m (θ_c), deg	K_{tb}	θ_m (θ_c), deg	K_{tb}	θ_m (θ_c), deg	K_{tb}	θ_m (θ_c), deg	K_{tb}	θ_m (θ_c), deg	K_{tb}	θ_m (θ_c), deg
2	2.20	94 (90)	4.37	90 (86)	3.45	0 (86)	3.33	90 (83)	[a]2.20	45 (93)	2.28	98 (89)
3	1.56	90 (87)	3.29	90 (84)	2.67	0 (84)	2.49	90 (82)	1.92	45 (85)	1.53	94 (86)
5	1.22	90 (84)	2.69	90 (82)	2.24	0 (84)	2.05	90 (82)	1.71	45 (83)	1.19	90 (83)
10	1.02	86 (83)	2.33	90 (82)	2.03	0 (84)	1.78	90 (82)	1.57	45 (82)	0.97	90 (83)
20	0.94	86 (83)	2.16	90 (82)	1.98	0 (84)	1.66	90 (82)	1.53	45 (82)	0.90	86 (83)
b_∞	[c]0.87	86 (83)	[c]2.00	90 (82)	[c]1.97	0 (84)	[c,d]1.53	90 (82)	[c]1.48	45 (82)	[c]0.82	86 (83)

[a] $(\sigma_{\theta\theta})_{max} = 2.40$ at $\theta = 120^\circ$. (See fig. 8.)
[b] An approximation using w/d = 20; see case 3 loading in appendix.
[c] $K_{tb} = (K_{tb})_\infty$.
[d] $(\sigma_{\theta\theta})_{max} = 1.65$ at $\theta = 0^\circ$. (See fig. 7.)

TABLE III.- TENSION STRESS-CONCENTRATION FACTORS FOR e/d RANGE WITH w/d = 20

e/d	Quasi-isotropic $[0^o/\pm45^o/90^o]_s$		0^o		90^o		$[0^o/90^o]_s$		$[\pm45^o]_s$		$[0^o/\pm45^o]_s$	
	K_{tb}	θ_m (θ_c), deg	K_{tb}	θ_m (θ_c), deg	K_{tb}	θ_m (θ_c), deg	K_{tb}	θ_m (θ_c), deg	K_{tb}	θ_m (θ_c), deg	K_{tb}	θ_m (θ_c), deg
1	1.86	79 (82)	6.45	90 (81)	3.00	0 (85)	3.60	90 (81)	2.90	45 (81)	2.10	78 (79)
2	1.25	86 (83)	3.96	90 (82)	2.14	0 (84)	2.54	90 (82)	1.94	45 (82)	1.25	86 (81)
3	1.09	86 (83)	3.04	90 (82)	2.00	0 (84)	2.13	90 (82)	1.72	45 (82)	1.08	86 (83)
5	1.00	86 (83)	2.55	90 (82)	1.96	0 (84)	1.85	90 (82)	1.60	45 (82)	0.96	86 (83)
10	0.94	86 (83)	2.16	90 (82)	1.98	0 (84)	1.66	90 (82)	1.53	45 (82)	0.90	86 (83)
a_∞	[b]0.87	86 (83)	[b]2.00	90 (82)	[b]1.97	0 (84)	[b,c]1.53	90 (82)	[b]1.48	45 (82)	[b]0.82	86 (83)

[a]An approximation using e/d = 10; see case 3 loading in appendix.
[b]$K_{tb} = (K_{tb})_\infty$.
[c]$(\sigma_{\theta\theta})_{max} = 1.65$ at $\theta = 0^o$. (See fig. 7.)

TABLE IV.- SHEAR STRESS-CONCENTRATION FACTORS FOR SHEAR-OUT PLANE WITH e/d RANGE AND w/d = 20

e/d	Quasi-isotropic $[0^o/\pm45^o/90^o]_s$		0^o		90^o		$[0^o/90^o]_s$		$[\pm45^o]_s$		$[0^o/\pm45^o]_s$	
	K_{sb}	$(x/R)^a$	K_{sb}	x/R	K_{sb}	x/R	K_{sb}	x/R	K_{sb}	x/R	K_{sb}	x/R
1	0.80	0.75	0.70	0.80	0.78	0.65	0.72	0.80	0.92	0.55	0.78	0.60
2	0.55	0.75	0.39	0.90	0.64	0.60	0.46	0.80	0.66	0.60	0.50	0.75
3	0.51	0.75	0.30	1.0	0.62	0.60	0.40	0.80	0.60	0.60	0.46	0.80
5	0.47	0.75	0.26	1.0	0.60	0.60	0.37	0.80	0.57	0.60	0.43	0.80
10	0.46	0.75	0.24	1.0	0.59	0.60	0.35	0.80	0.55	0.60	0.42	0.80
b_∞	$^c0.45$	0.75	$^c0.24$	1.0	$^c0.57$	0.60	$^c0.33$	0.80	$^c0.52$	0.65	$^c0.41$	0.85

[a]Location of peak shear stress on shear-out plane (y = R).
[b]An approximation using e/d = 10; see case 3 loading in appendix.
[c]$K_{sb} = (K_{sb})_\infty$.

TABLE V.- STRESS-CONCENTRATION FACTORS FOR A SQUARE QUASI-ISOTROPIC LAMINATE LOADED BY A RIGID PIN; $\theta_c = 83^o$

w/d	Remote loading type[a]					
	Tension (case 1)		Compression (case 2)		Tension/compression (case 3)	
	K_{tb}	θ_m, deg	K_{tb}	θ_m, deg	K_{tb}	θ_m, deg
3	1.832 [b](1.728)	90	0.576 [b](0.542)	82	1.157 [b](1.144)	90
5	1.304 [b](1.283)	90	0.693 [b](0.645)	82	0.964	86
10	1.040	86	0.752 [b](0.736)	82	0.888	86
15	0.975	86	0.777 [b](0.774)	82	0.874	86
20	0.944	86	0.794	86	0.869	86

[a]See figure 22 for description of loading types.
[b]Stress concentration at $\theta = 86^o$.

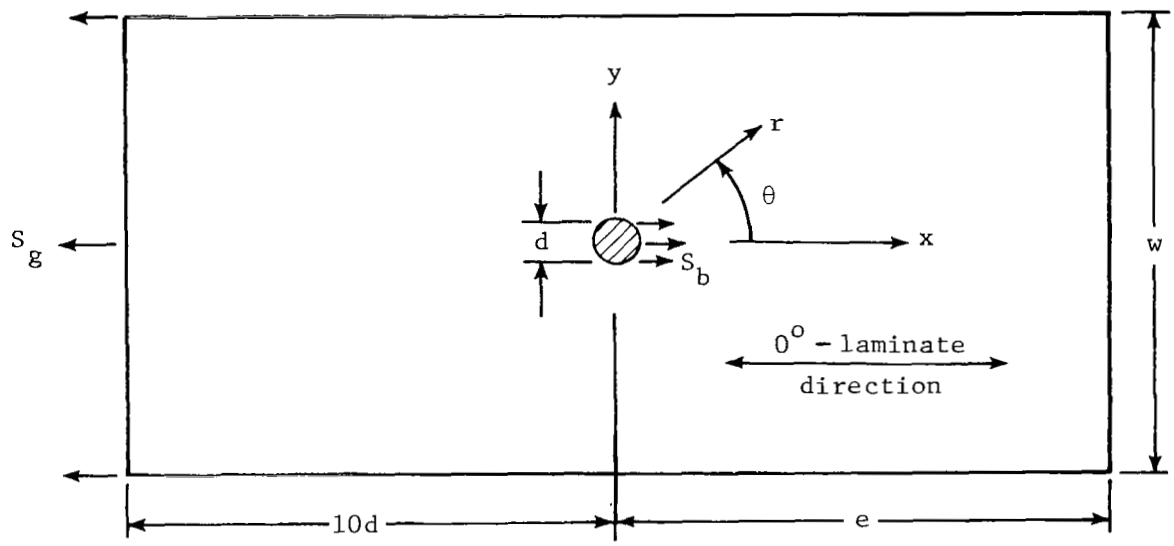

Figure 1.- Laminate configuration and loading.

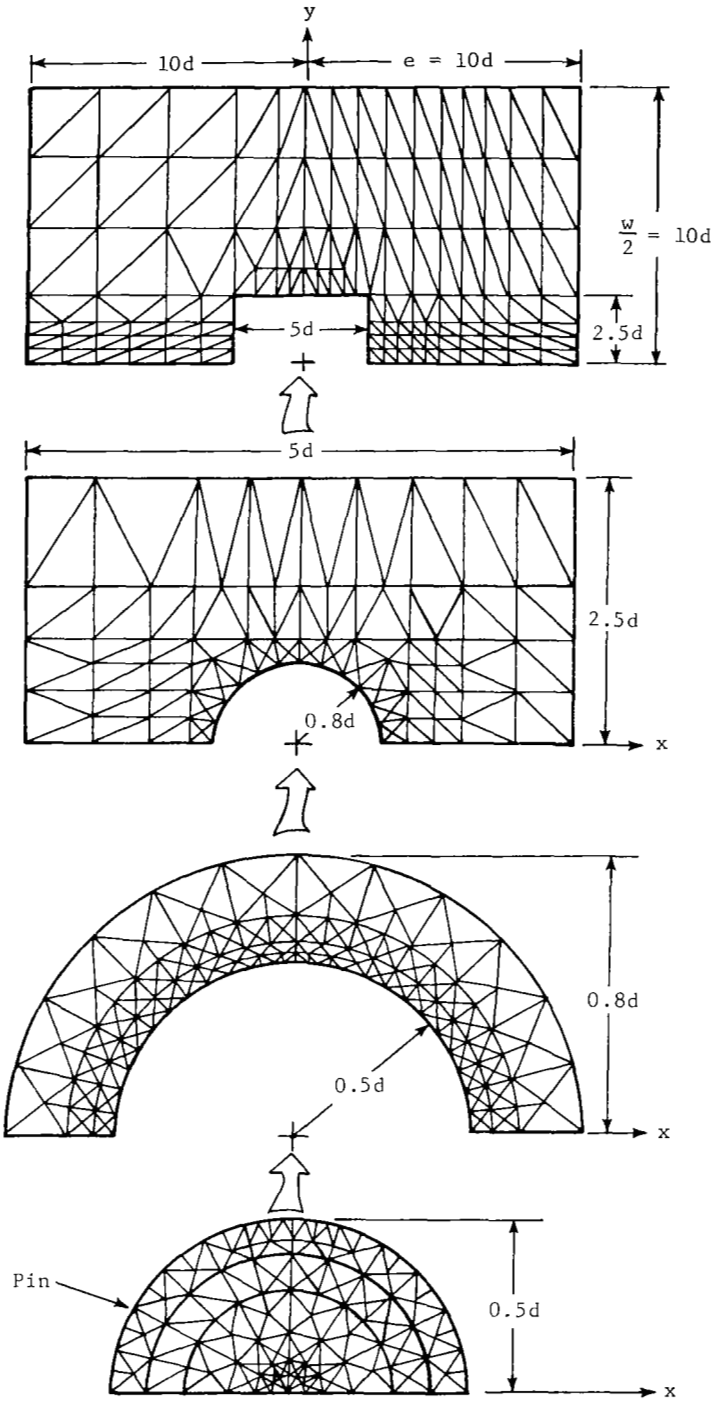

Figure 2.- Finite-element model.

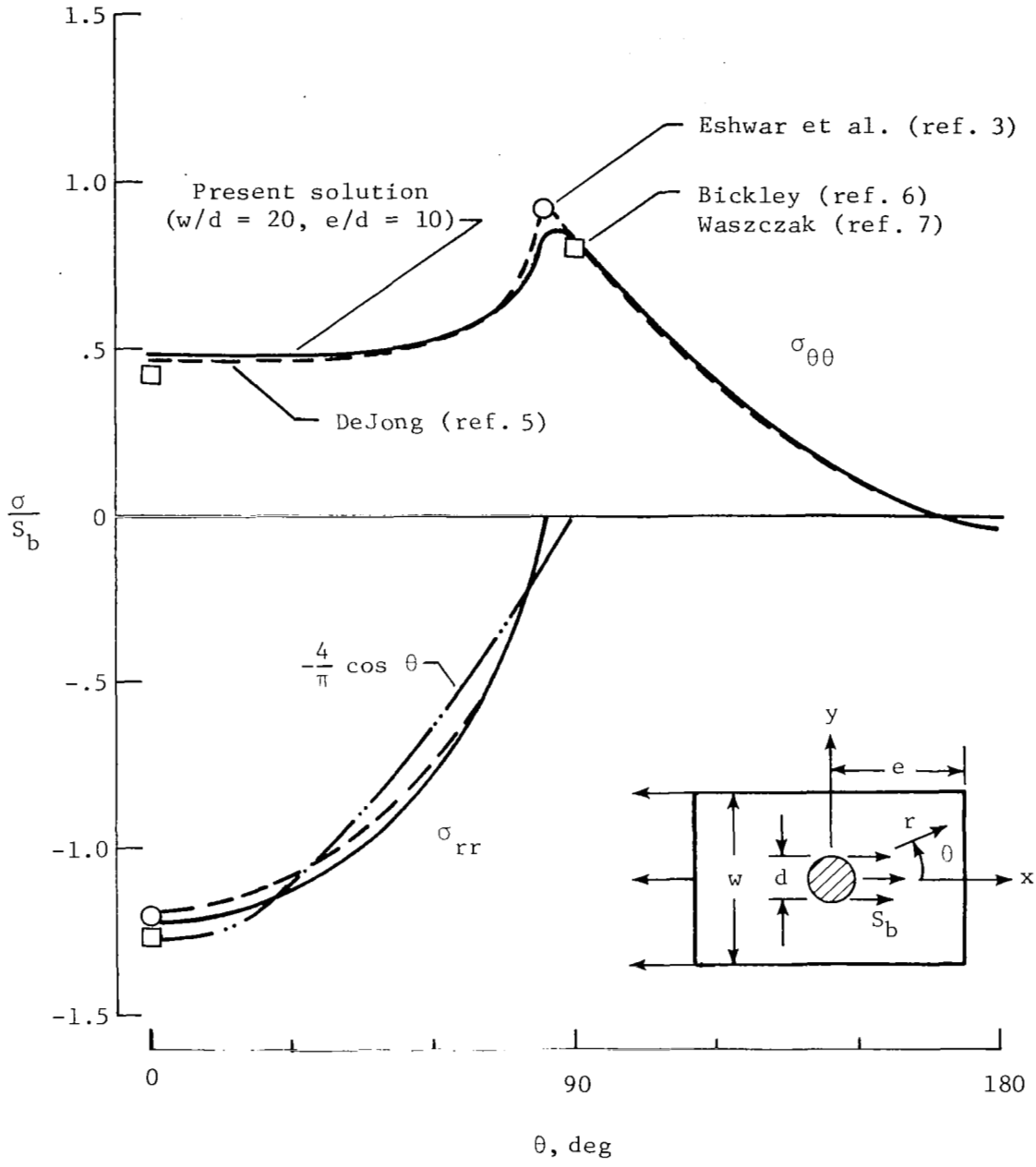

Figure 3.- Stresses in quasi-isotropic laminate loaded by a rigid pin; w/d = 20, e/d = 10.

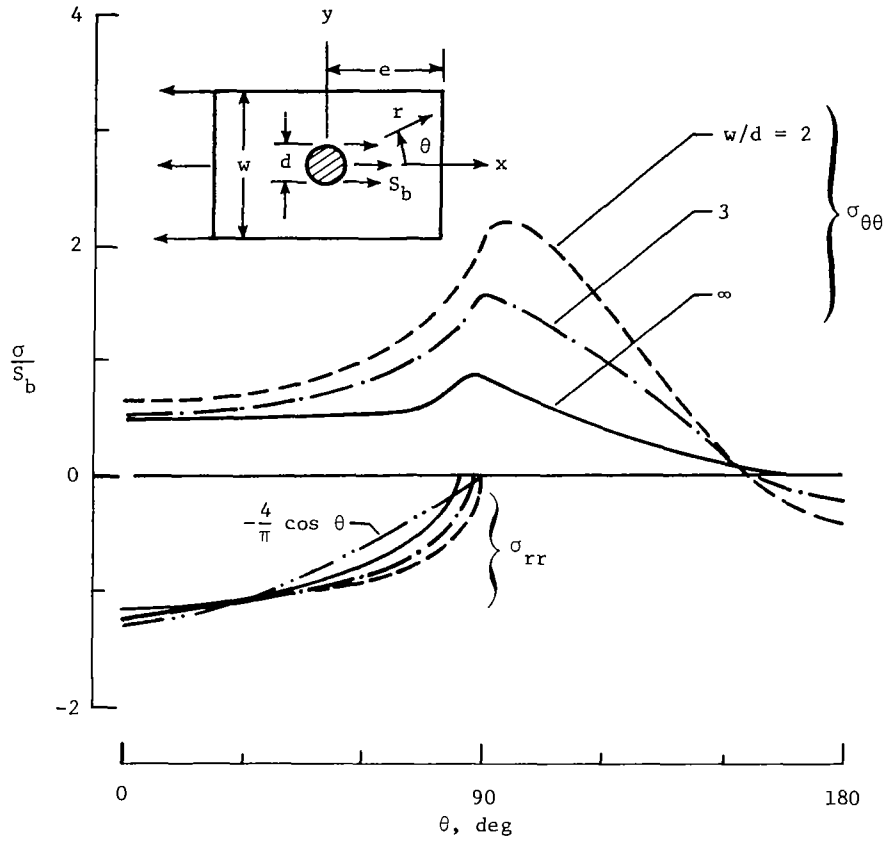

(a) Stresses along hole boundary (r = R).

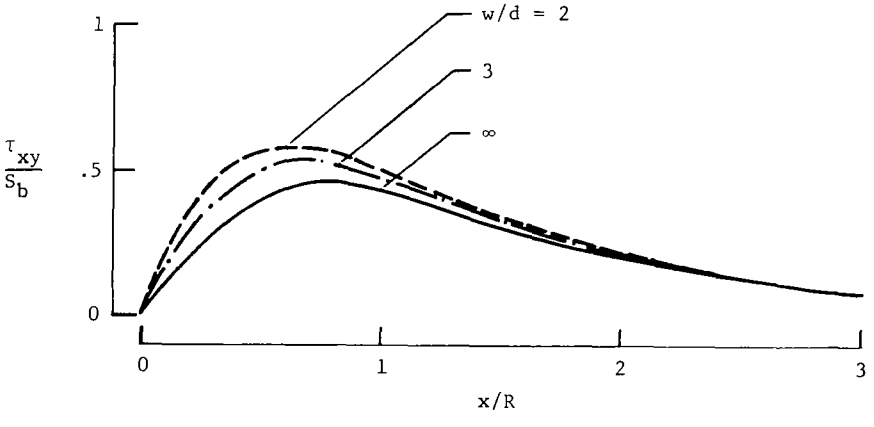

(b) Shear stress along shear-out plane (y = R).

Figure 4.- Stresses in quasi-isotropic laminate as a function of w/d; e/d = 10.

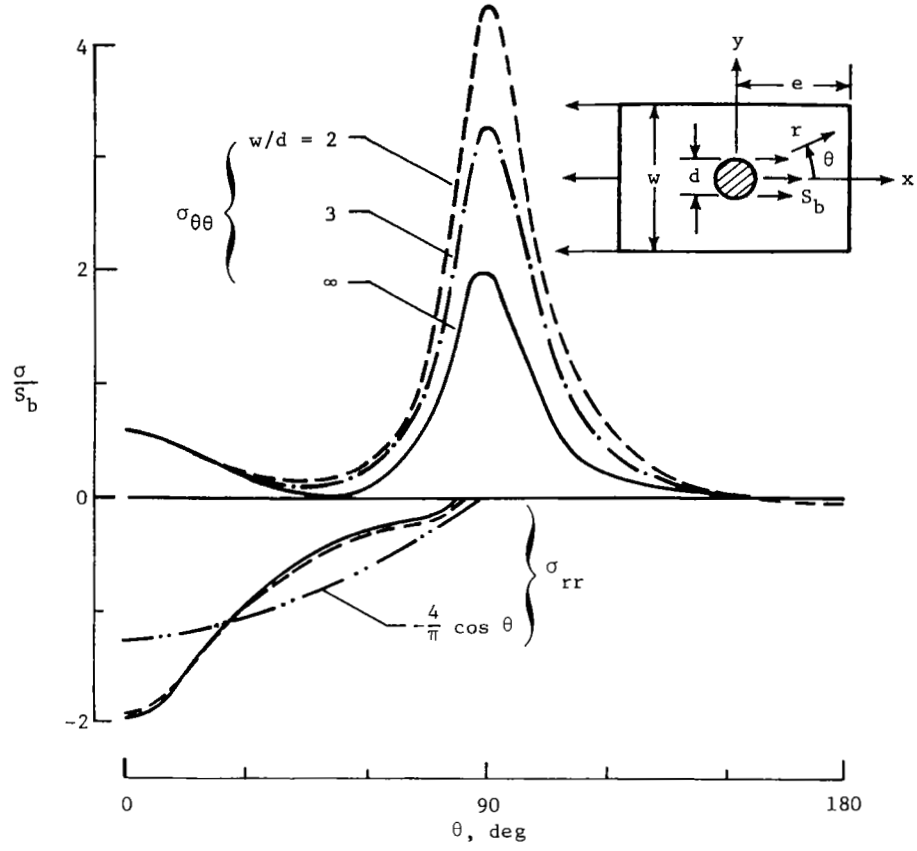

(a) Stresses along hole boundary (r = R).

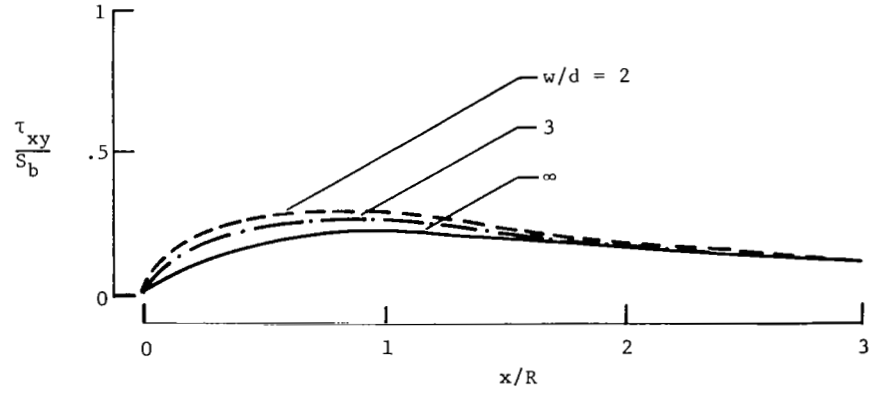

(b) Shear stress along shear-out plane.

Figure 5.- Stresses in 0° laminate as a function of w/d; e/d = 10.

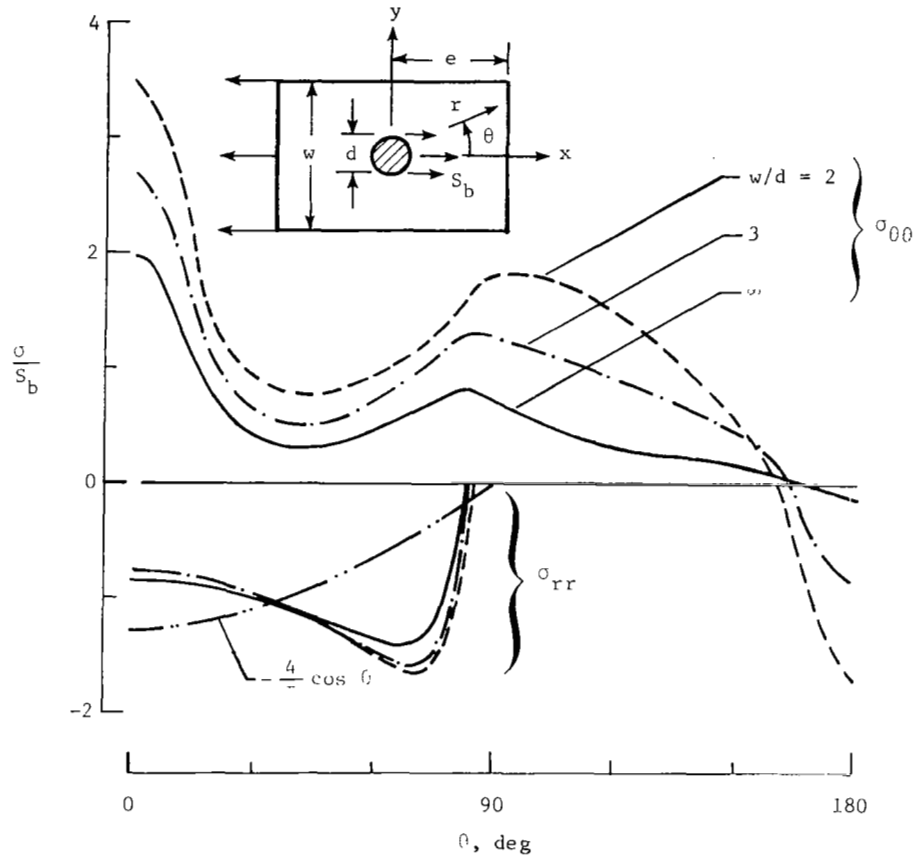

(a) Stresses along hole boundary (r = R).

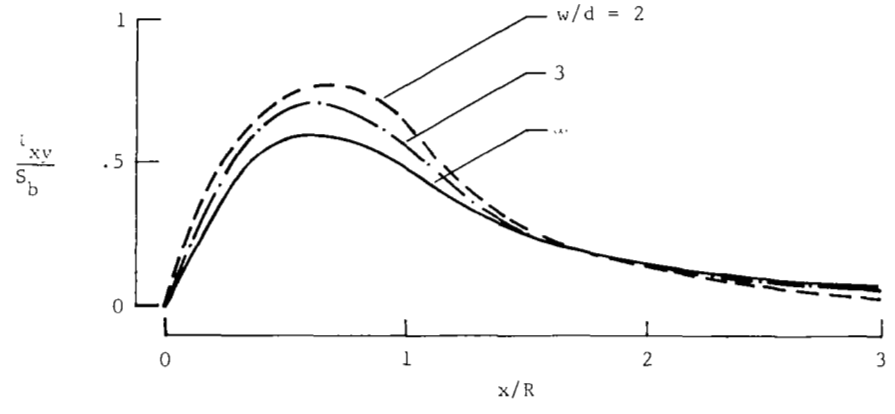

(b) Shear stress along shear-out plane (y = R).

Figure 6.- Stresses in 90° laminate as a function of w/d; e/d = 10.

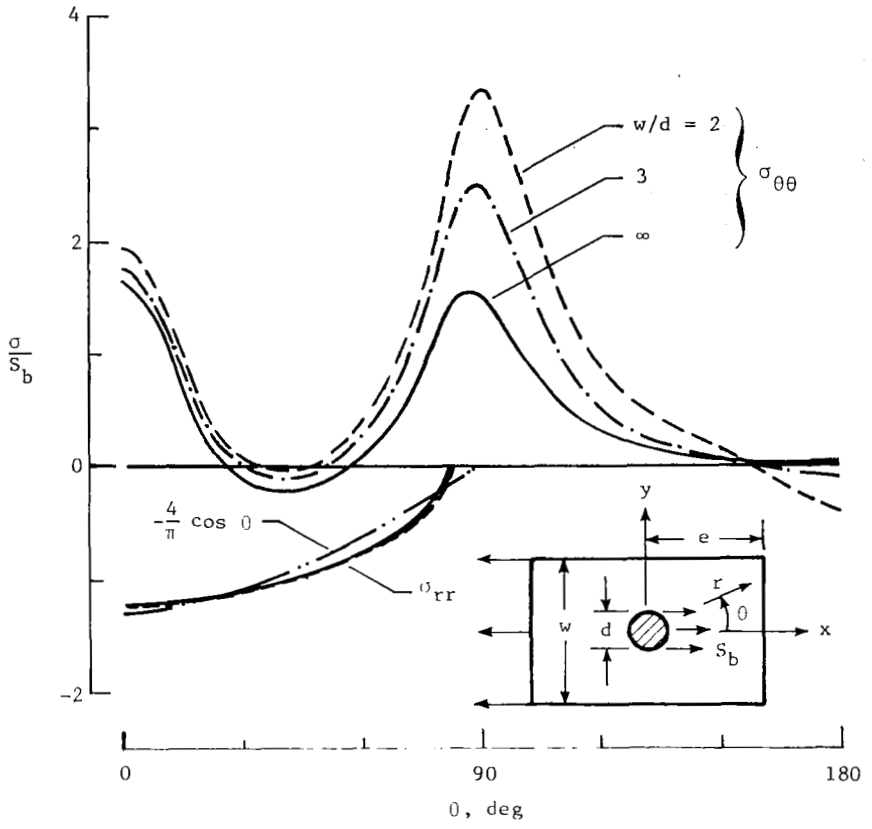

(a) Stresses along hole boundary (r = R).

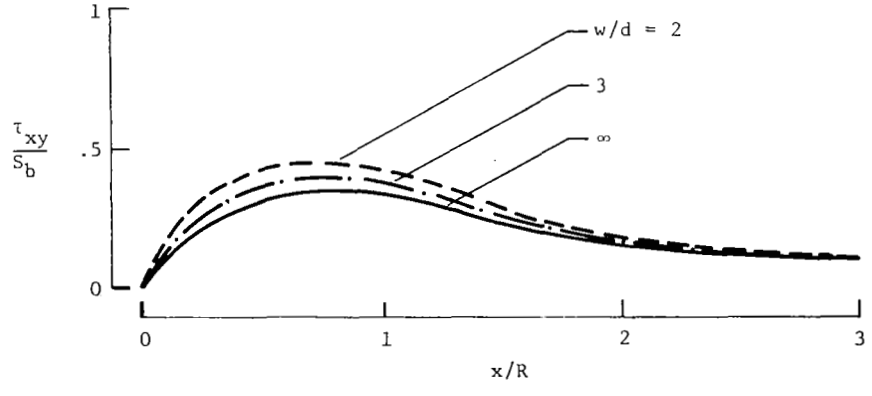

(b) Shear stress along shear-out plane (y = R).

Figure 7.- Stresses in $[0^o/90^o]_s$ laminate as a function of w/d; e/d = 10.

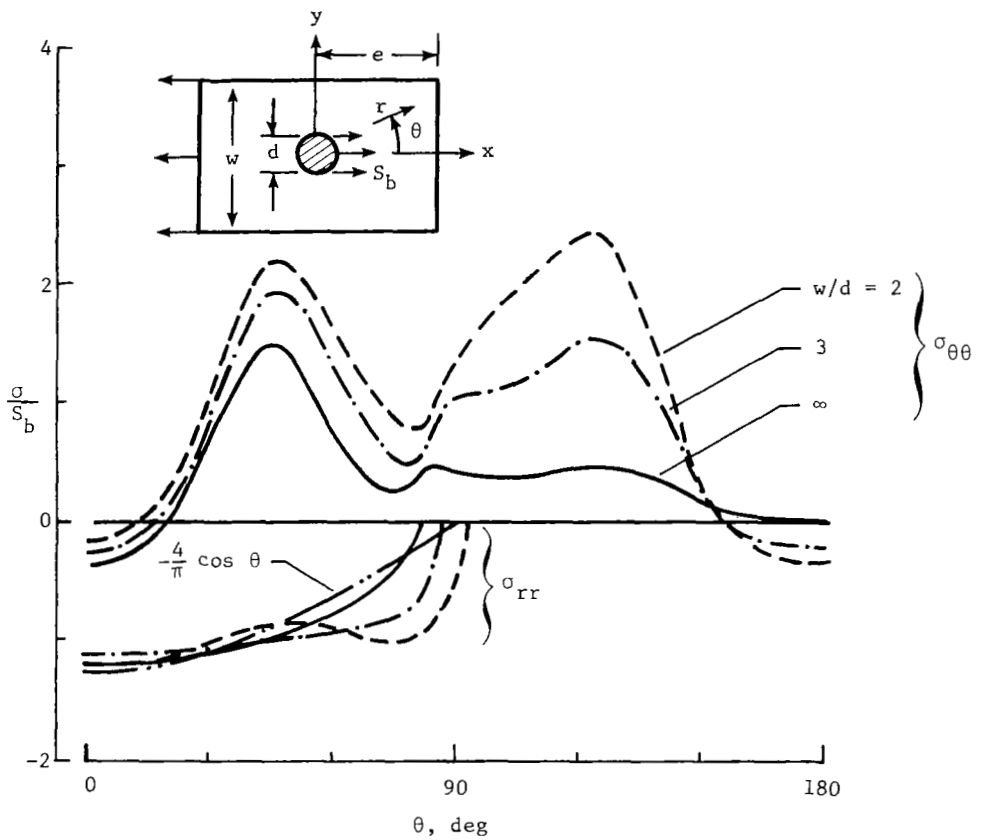

(a) Stresses along hole boundary (r = R).

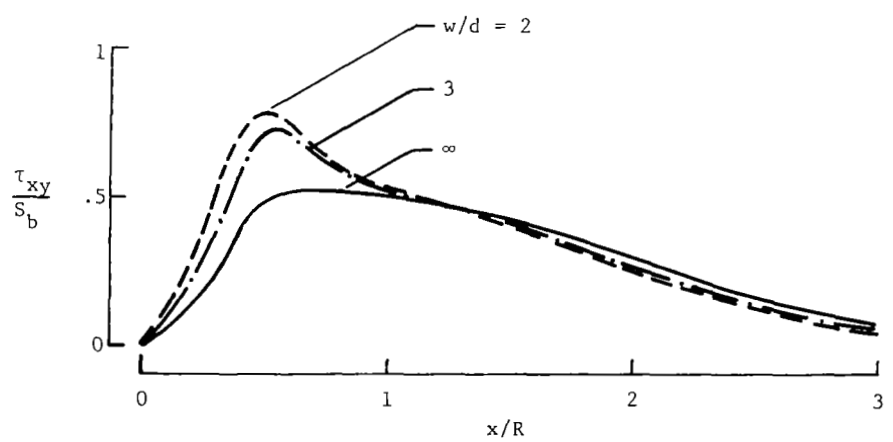

(b) Shear stress along shear-out plane (y = R).

Figure 8.- Stresses in $[\pm 45^{o}]_s$ laminate as a function of w/d; e/d = 10.

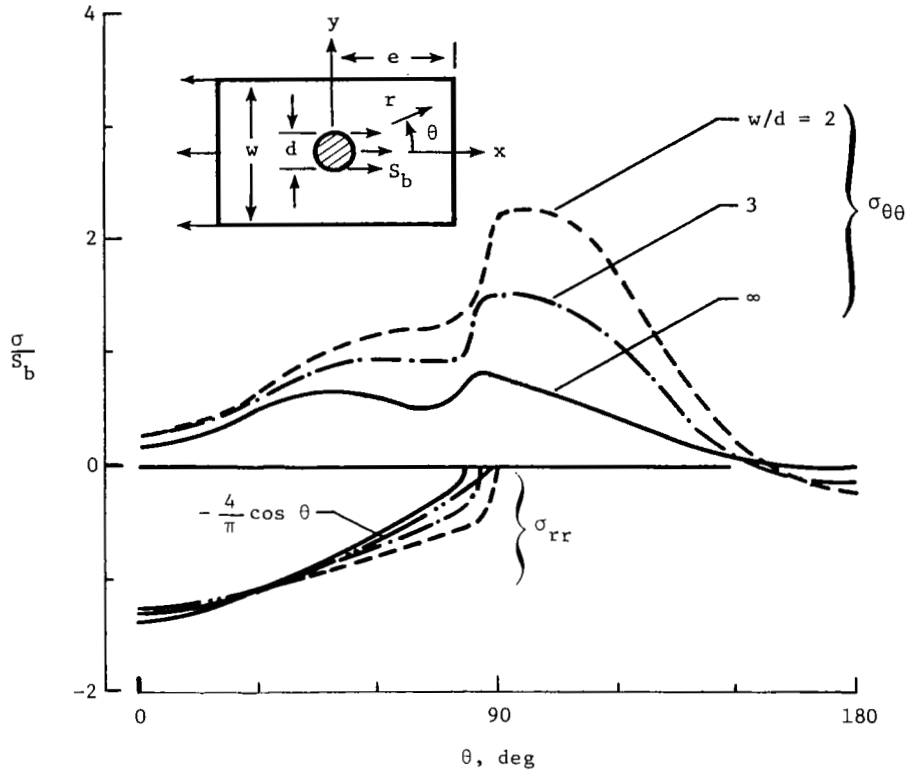

(a) Stresses along hole boundary (r = R).

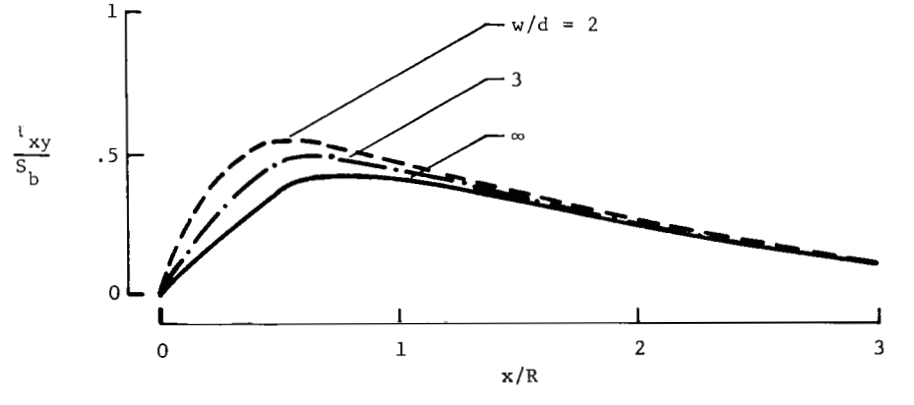

(b) Shear stress along shear-out plane (y = R).

Figure 9.- Stresses in $[0^o/45^o]_s$ laminate as a function of w/d; e/d = 10.

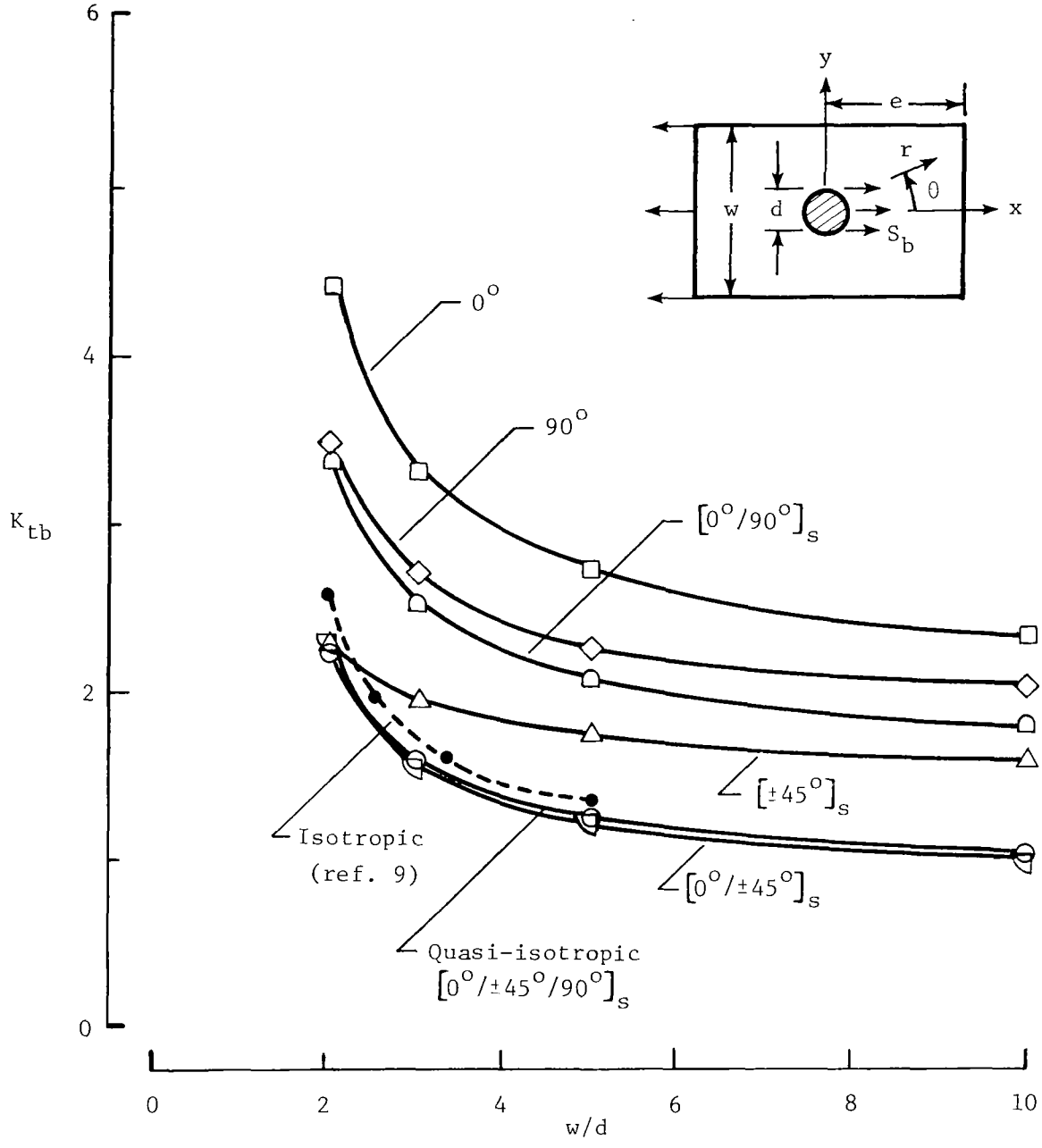

Figure 10.- $\sigma_{\theta\theta}$ stress-concentration factors as a function of w/d; e/d = 10.

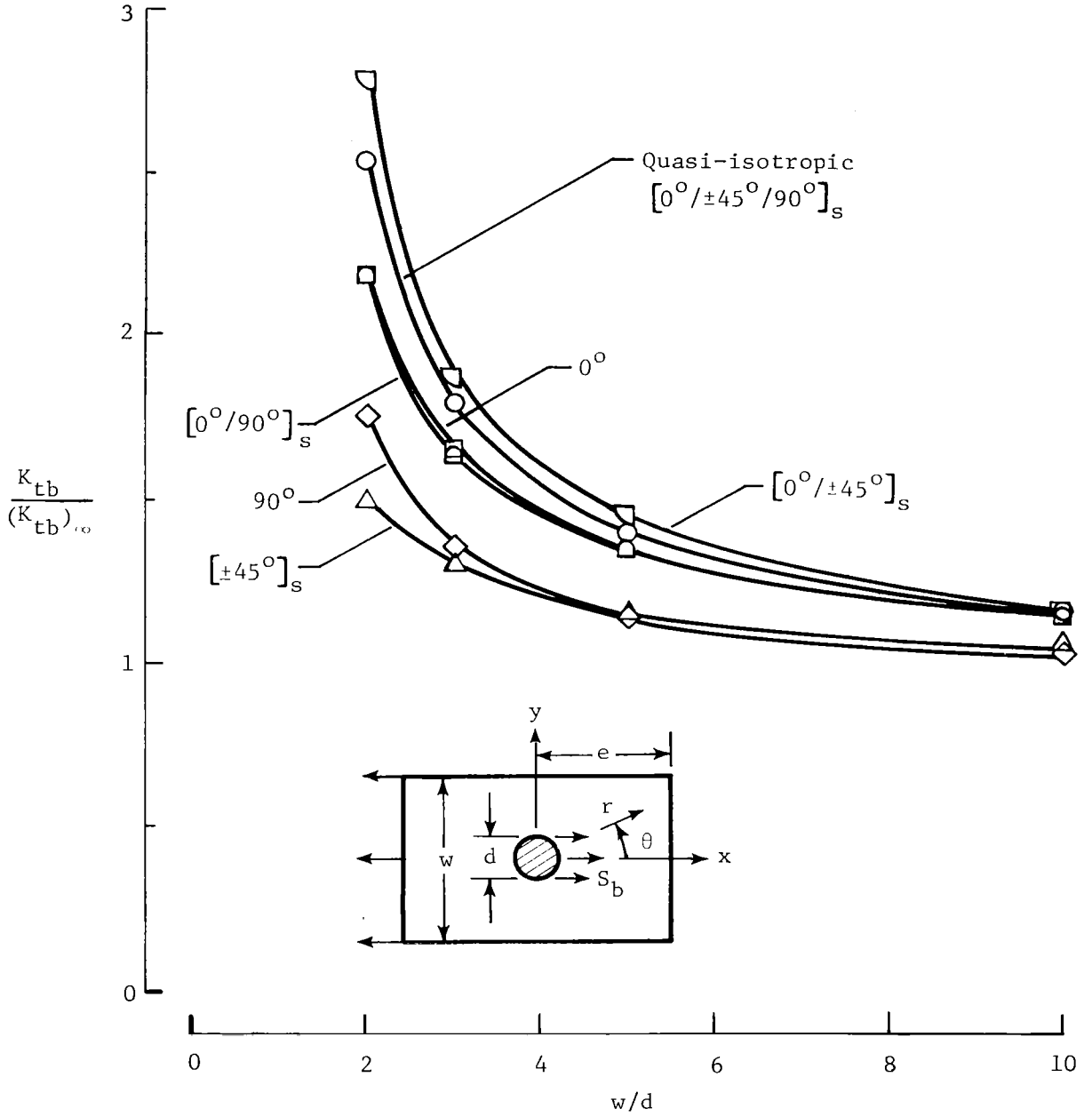

Figure 11.- Normalized $\sigma_{\theta\theta}$ stress-concentration factors as a function of w/d; e/d = 10.

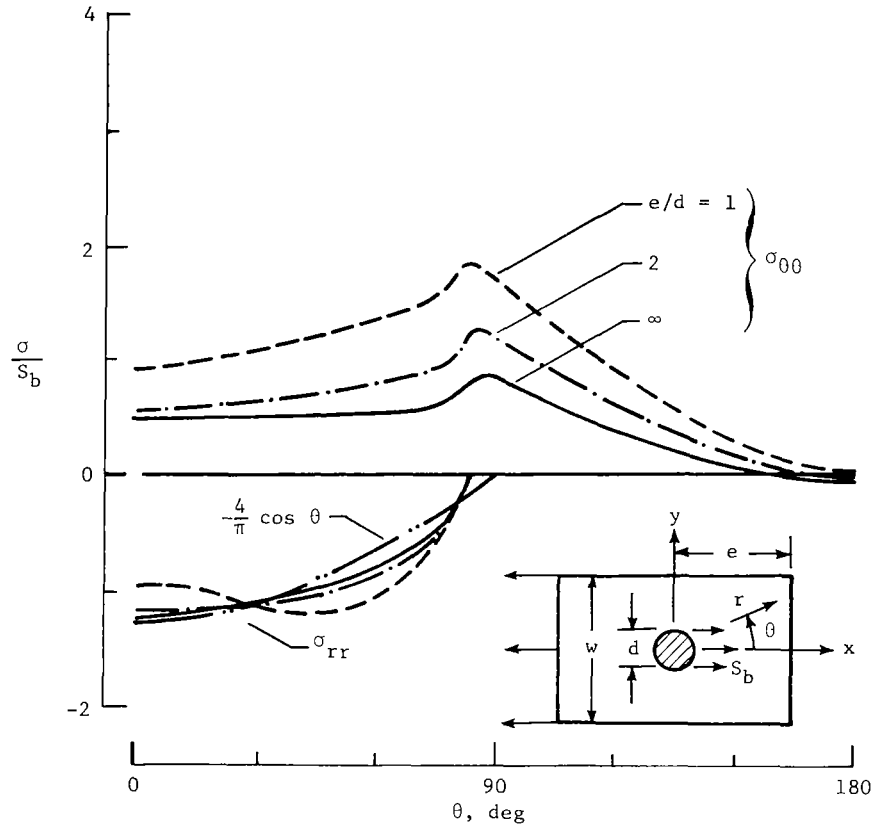

(a) Stresses along hole boundary.

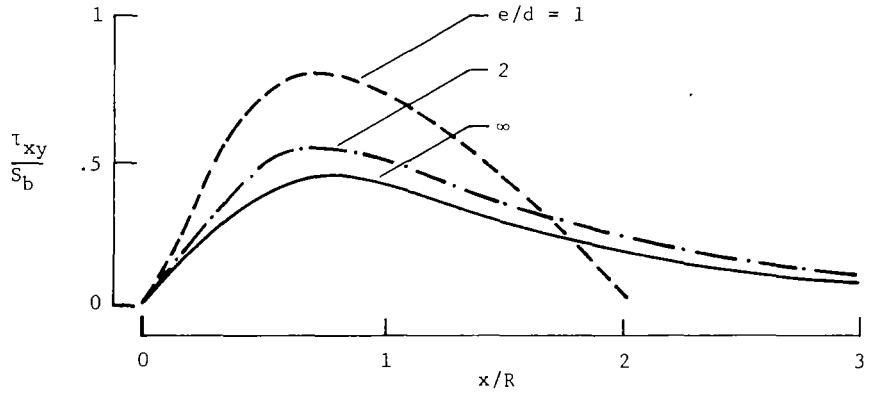

(b) Shear stress along shear-out plane (y = R).

Figure 12.- Stresses in quasi-isotropic laminate as a function of e/d; w/d = 20.

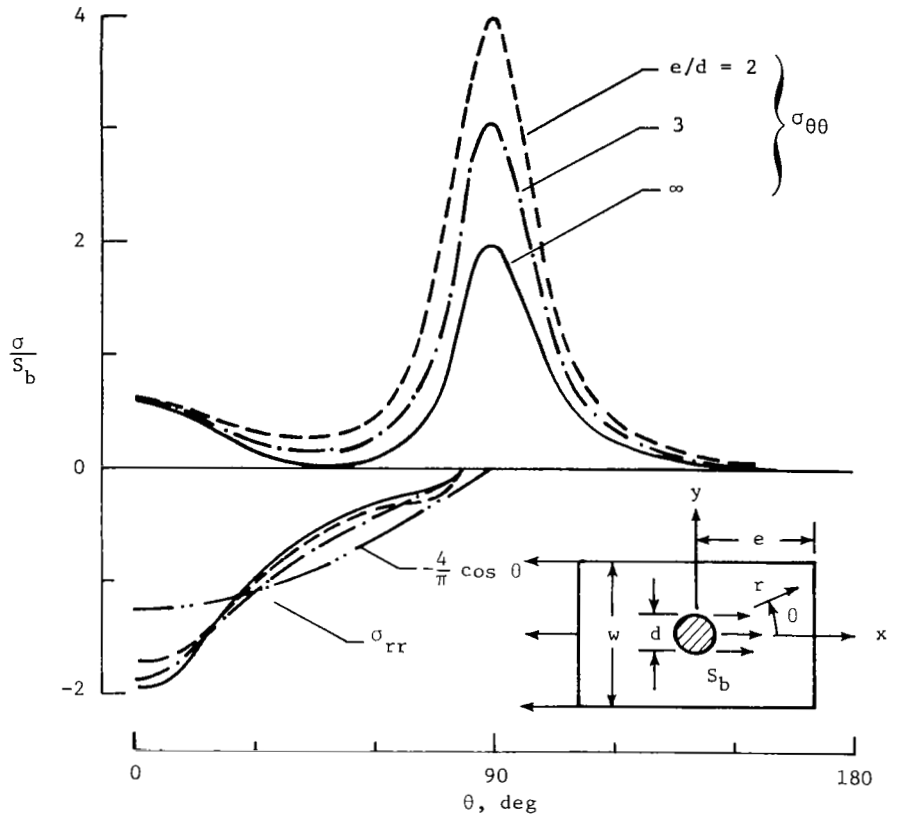

(a) Stresses along hole boundary.

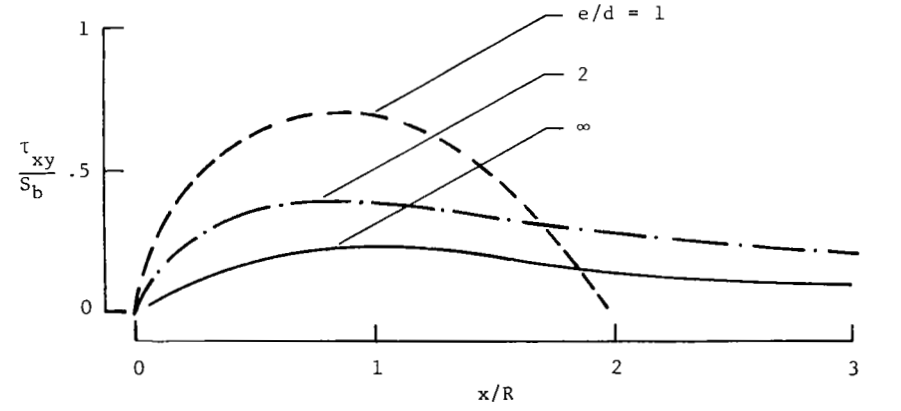

(b) Shear stress along shear-out plane (y = R).

Figure 13.- Stresses in 0^o laminate as a function of e/d; w/d = 20.

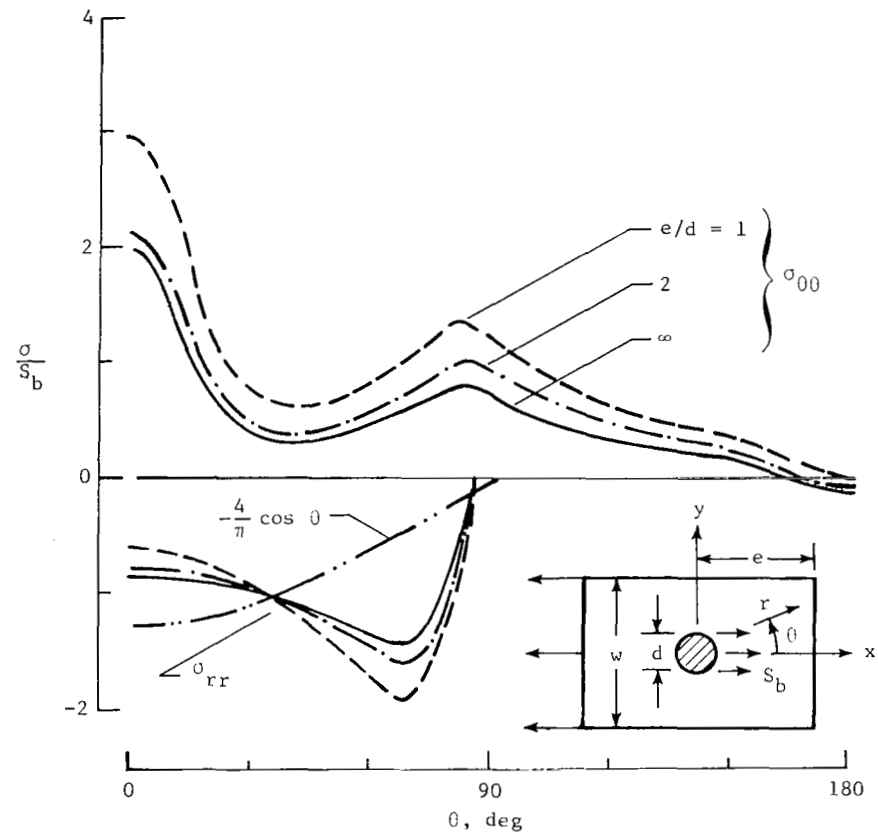

(a) Stresses along hole boundary.

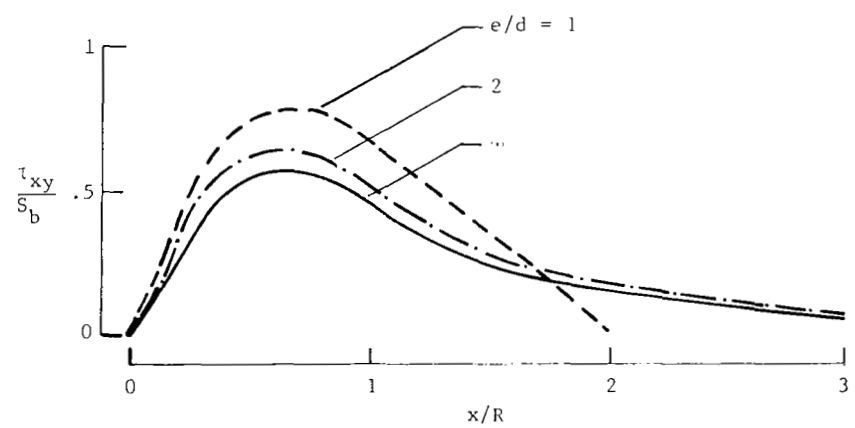

(b) Shear stress along shear-out plane (y = R).

Figure 14.- Stresses in 90° laminate as a function of e/d; w/d = 20.

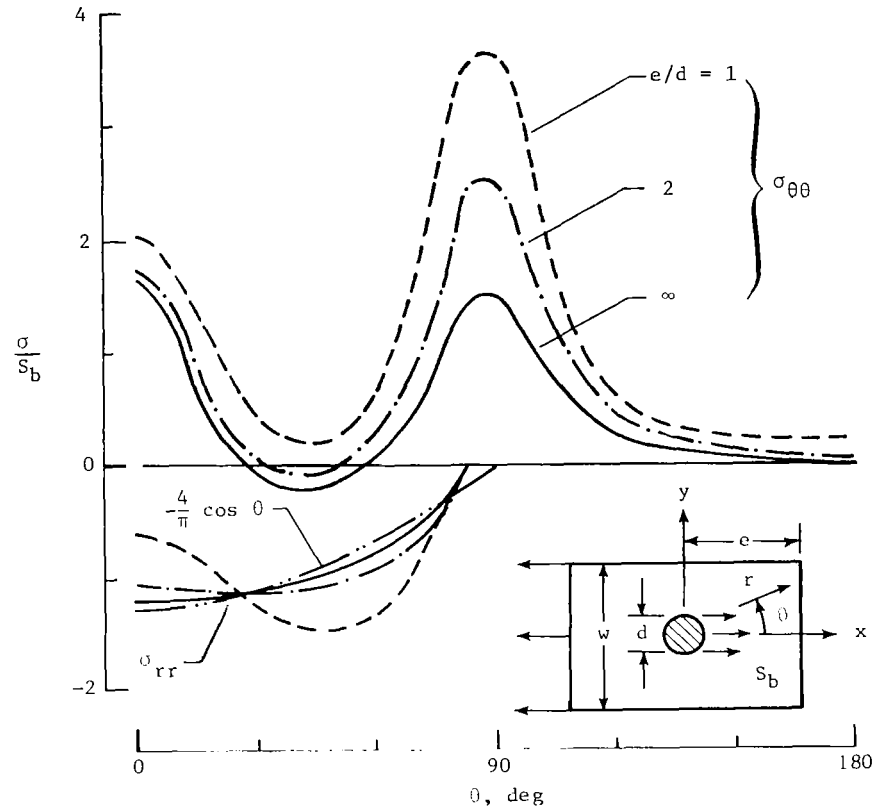

(a) Stresses along hole boundary.

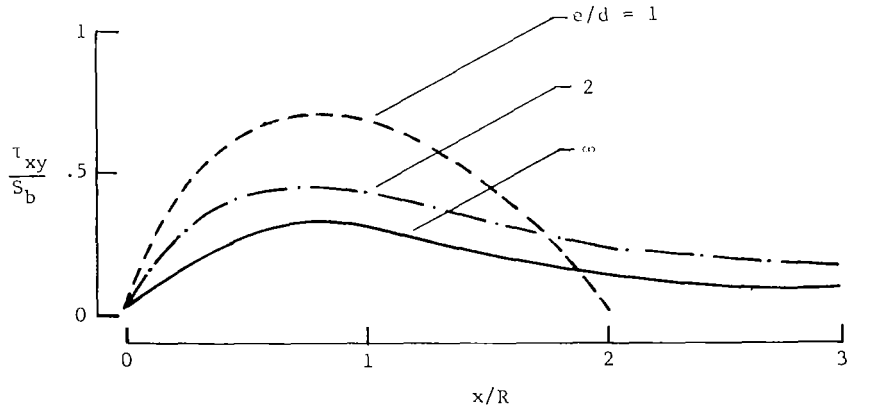

(b) Shear stress along shear-out plane (y = R).

Figure 15.- Stresses in $[0^o/90]_s$ laminate as a function of e/d; w/d = 20.

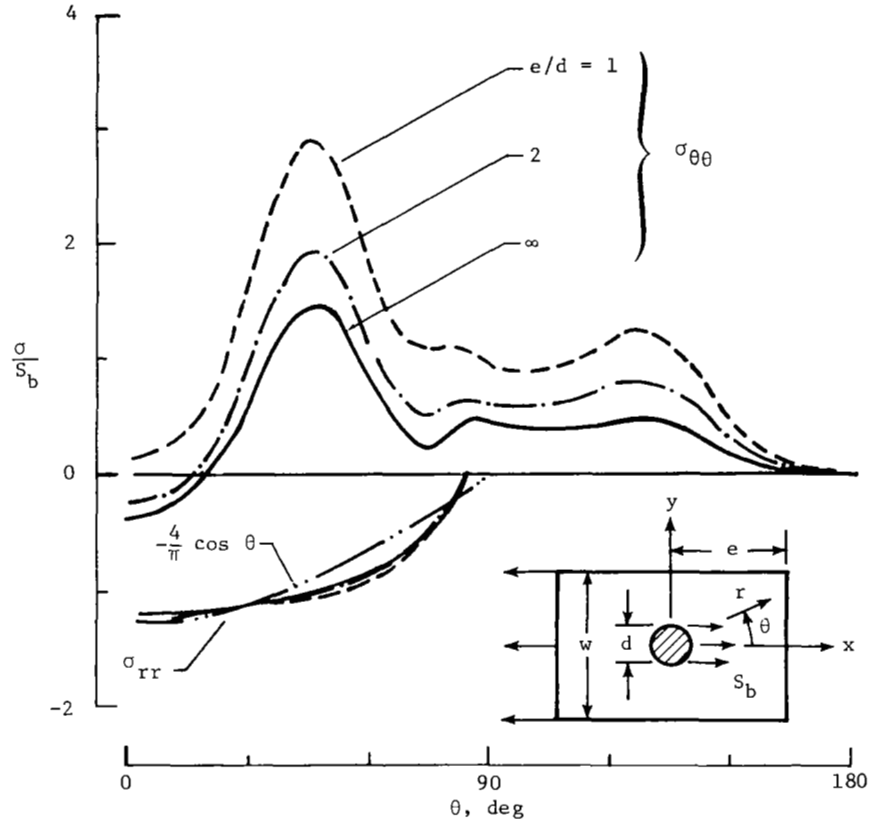

(a) Stresses along hole boundary.

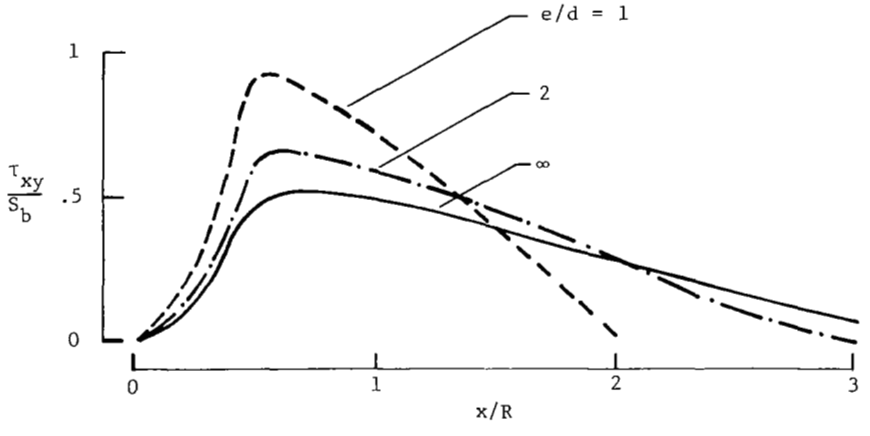

(b) Shear stress along shear-out plane (y = R).

Figure 16.- Stresses in $[\pm 45^{o}]_s$ laminate as a function of e/d; w/d = 20.

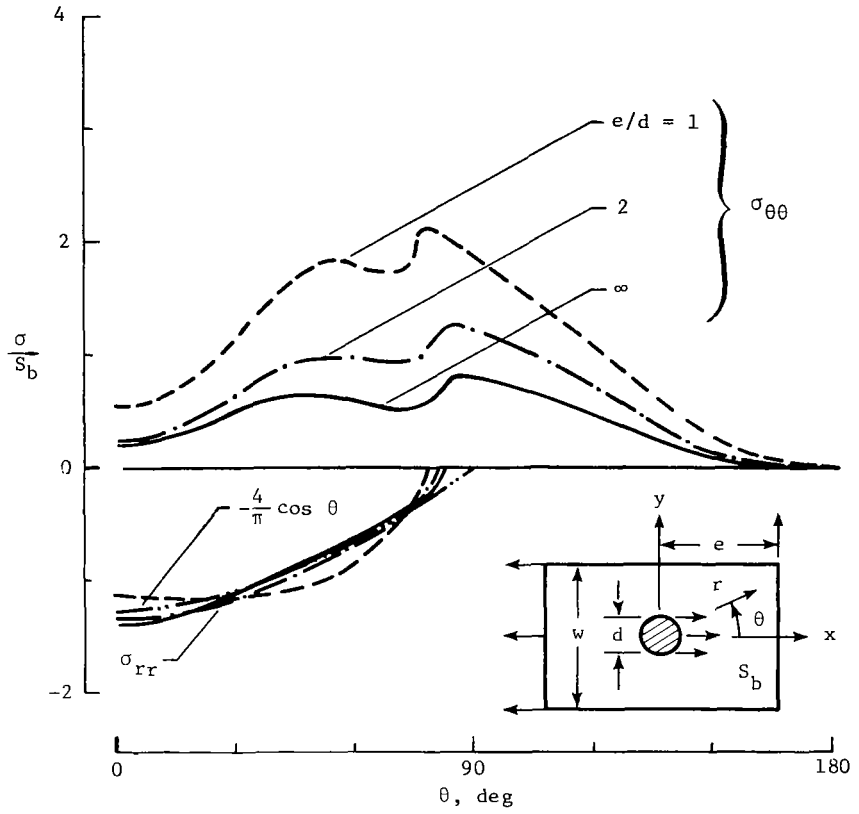

(a) Stresses along hole boundary.

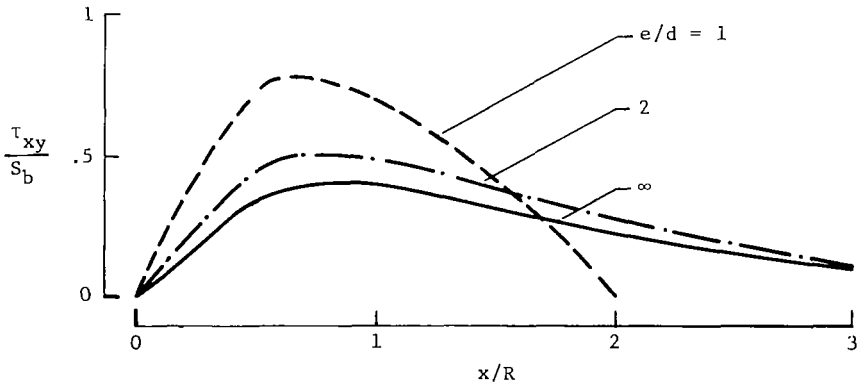

(b) Shear stress along shear-out plane (y = R).

Figure 17.- Stresses in $[0^o/\pm45^o]_s$ laminate as a function of e/d; w/d = 20.

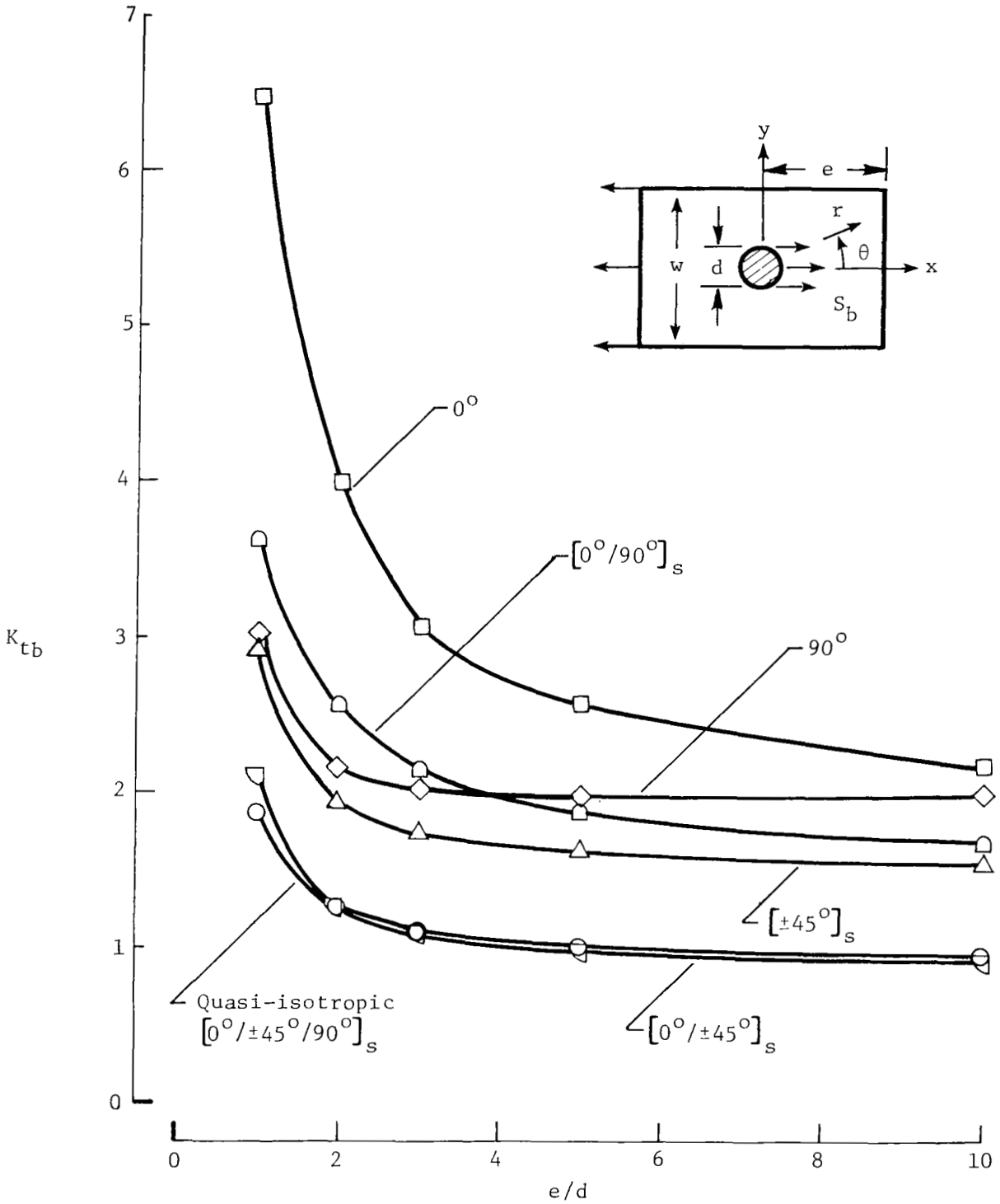

Figure 18.- $\sigma_{\theta\theta}$ stress-concentration factors as a function of e/d; w/d = 20.

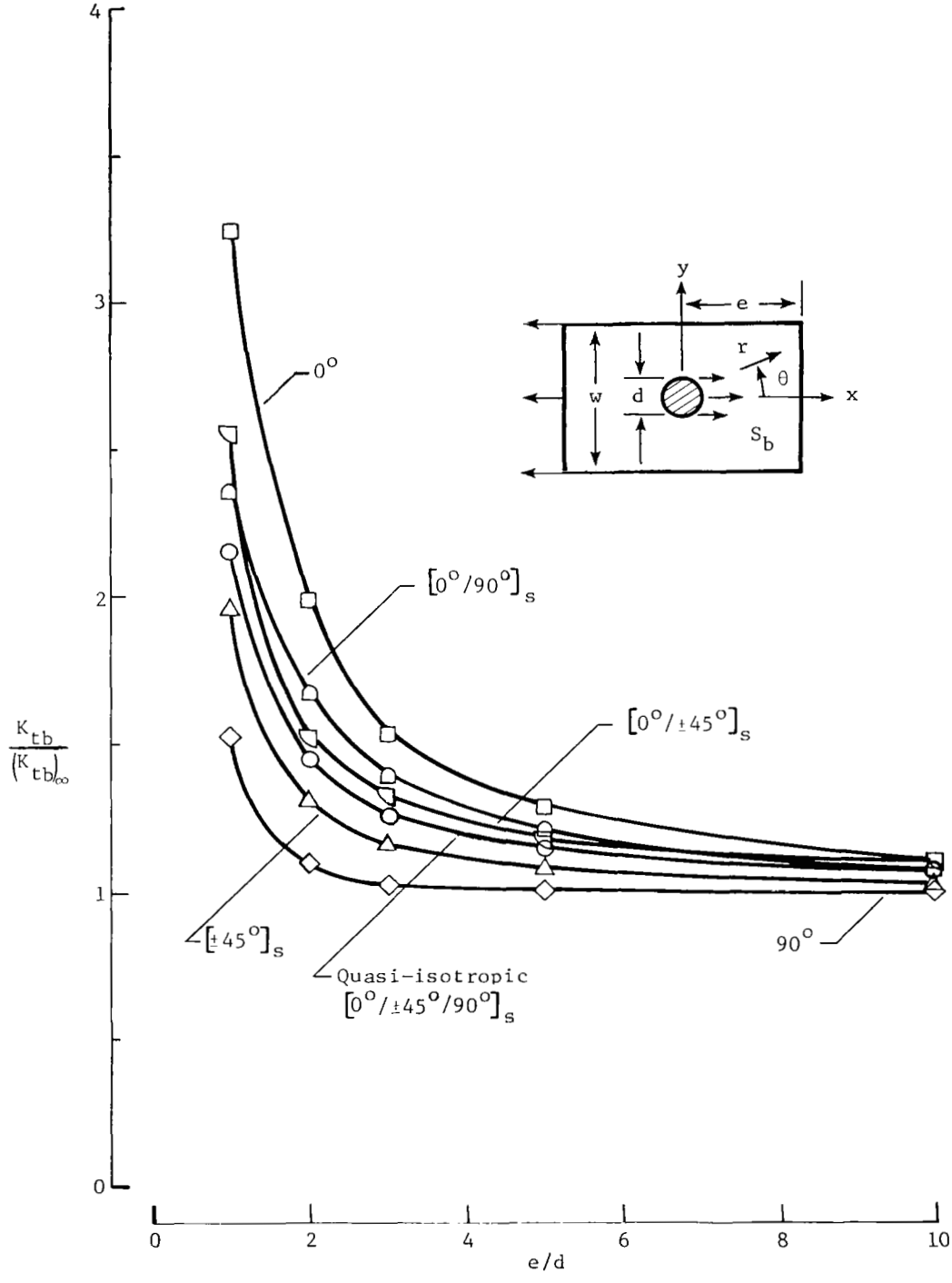

Figure 19.- Normalized $\sigma_{\theta\theta}$ stress-concentration factors as a function of e/d; w/d = 20.

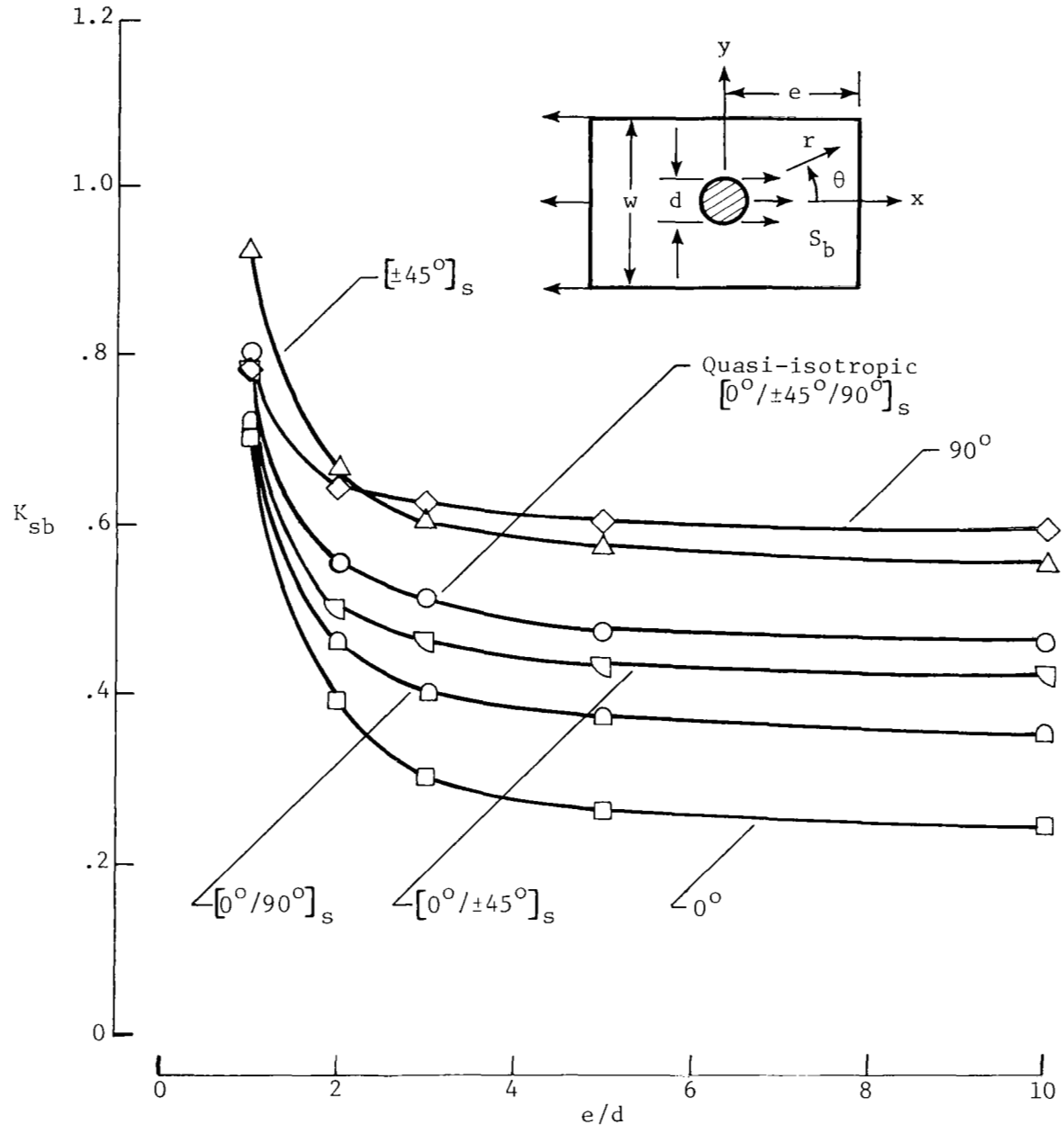

Figure 20.- τ_{xy} stress-concentration factors for shear-out plane (y = R); w/d = 20.

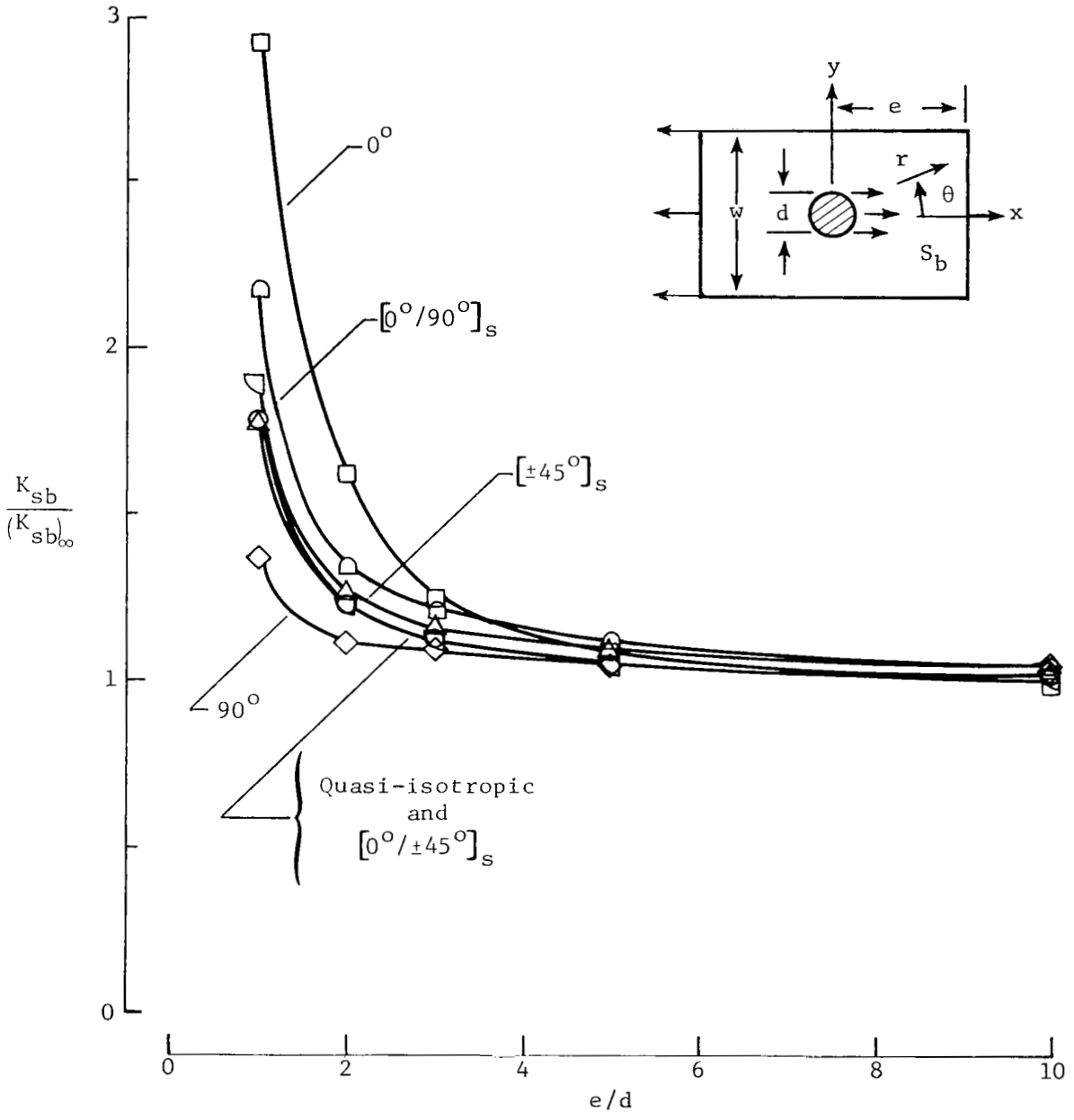

Figure 21.- Normalized τ_{xy} stress-concentration factors for shear-out plane (y = R); w/d = 20.

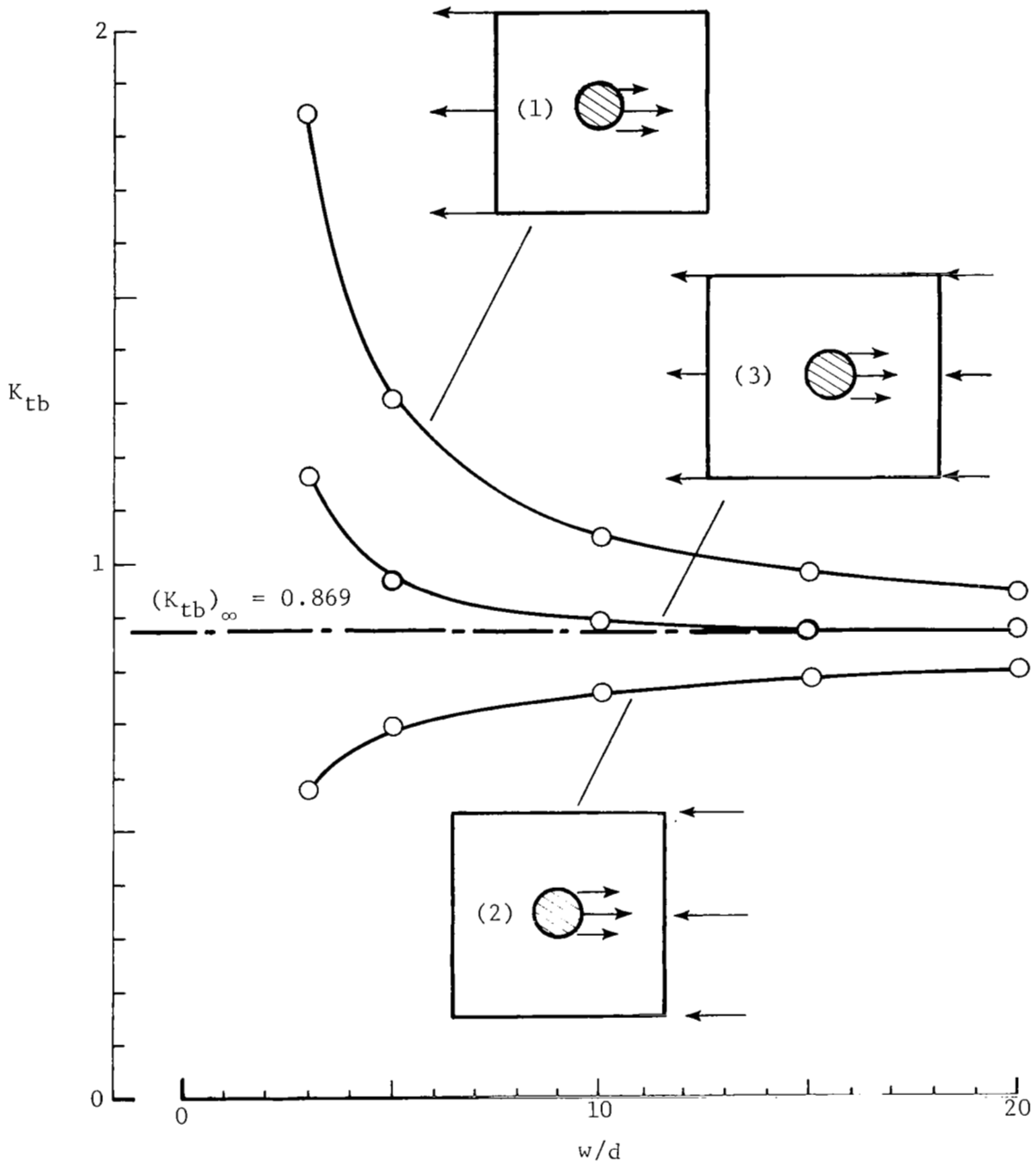

Figure 22.- $\sigma_{\theta\theta}$ stress-concentration factors for a square quasi-isotropic laminate loaded by a rigid pin.

1. Report No.	2. Government Accession No.	3. Recipient's Catalog No.
NASA TP-1862		

4. Title and Subtitle	5. Report Date
STRESS-CONCENTRATION FACTORS FOR FINITE ORTHOTROPIC LAMINATES WITH A PIN-LOADED HOLE	May 1981
	6. Performing Organization Code 506-53-23-05

7. Author(s)	8. Performing Organization Report No.
John H. Crews, Jr., C. S. Hong, and I. S. Raju	L-14300
	10. Work Unit No.

9. Performing Organization Name and Address	11. Contract or Grant No.
NASA Langley Research Center Hampton, VA 23665	
	13. Type of Report and Period Covered Technical Paper

12. Sponsoring Agency Name and Address	14. Sponsoring Agency Code
National Aeronautics and Space Administration Washington, DC 20546	

15. Supplementary Notes

John H. Crews, Jr.: Langley Research Center.
C. S. Hong: Former NRC-NASA Resident Research Associate, now at The Korea Institute of Science, Seoul, Korea.
I. S. Raju: Joint Institute for Advancement of Flight Sciences, The George Washington University, Hampton, Virginia.

16. Abstract

Stresses were calculated for finite-size orthotropic laminates loaded by a frictionless steel pin in a circular hole of the same diameter. These calculations were based on finite-element analyses for six laminates: quasi-isotropic $[0^\circ/\pm45^\circ/90^\circ]_s$, 0°, 90°, $[0^\circ/90^\circ]_s$, $[\pm45^\circ]_s$, and $[0^\circ/\pm45^\circ]_s$. Stress concentration factors, based on nominal bearing stress, were determined for wide ranges of the ratios of width to diameter w/d and edge distance to diameter e/d. An infinite-laminate case was also analyzed for each laminate. Orthotropy had a significant influence on the tensile stress concentration at the hole. For example, the stress-concentration factors for the infinite-laminate cases ranged from 0.82 to 2.16, compared with 0.87 for the quasi-isotropic laminate. The finite widths and edge distances strongly influenced the tensile stress concentration. For the practical range $w/d \geq 3$, the peak tensile stresses were as much as 80 percent larger than the infinite-laminate reference value. For $e/d \geq 3$, these stresses were amplified by as much as 50 percent. In contrast, the finite width and edge distance had little effect on shear-out and bearing stress concentrations.

17. Key Words (Suggested by Author(s))	18. Distribution Statement
Composites Finite width Orthotropic Stress-concentration factor Pin-loaded hole Elastic	Unclassified - Unlimited Subject Category 24

19. Security Classif. (of this report)	20. Security Classif. (of this page)	21. No. of Pages	22. Price
Unclassified	Unclassified	40	A03

For sale by the National Technical Information Service, Springfield, Virginia 22161

NASA-Langley, 1981